SYSTEMATIC INVESTIGATION OF WAVY SURFACE ROUGHNESS PROFILES USING COMMON ROUGHNESS ALGORITHMS

by

Russell Gray

A thesis

submitted in partial fulfillment

of the requirements for the degree of

Master of Science in Civil Engineering

Boise State University

August 2023

BOISE STATE UNIVERSITY GRADUATE COLLEGE

DEFENSE COMMITTEE AND FINAL READING APPROVALS

of the thesis submitted by

Russell Gray

Thesis Title: Systematic Investigation of Simulated Wavy Surface Roughness Profiles Using Common Roughness Algorithms

Date of Final Oral Examination: 12 June 2023

The following individuals read and discussed the thesis submitted by student Russell Gray, and they evaluated the student's presentation and response to questions during the final oral examination. They found that the student passed the final oral examination.

Nick Hudyma, Ph.D., PE	Chair, Supervisory Committee
Bhaskar Chittoori, Ph.D., PE	Member, Supervisory Committee
Mary McLaughlin, Ph.D., PE	Member, Supervisory Committee

The final reading approval of the thesis was granted by Nick Hudyma, Ph.D., Chair of the Supervisory Committee. The thesis was approved by the Graduate College.

ACKNOWLEDGMENTS

First, I would like to acknowledge the Civil Engineering Department and the Stellar Engineering Student Graduate Program Scholarship (SEnS GPS) for providing us with the academic and financial support that I would need to receive my Master of Science from Boise State University. Without the scholarship and the support of the faculty, I would not have taken this great opportunity.

I would like to offer my greatest acknowledgment to my graduate professor Dr. Nick Hudyma for being able and willing to help me at any time, even when times were busy for him. His support and expertise throughout this research made everything go smoothly, as I found times when I would want to give up. His enthusiasm and passion for Geotechnical Engineering kept me motivated in times when I lacked motivation and has instilled a growing passion in me to be the best Geotechnical Engineer that I can be.

I would also like to acknowledge the faculty at Boise State University, as they provided me with the skills and knowledge to be able to conduct research and put together a thesis. Their willingness to help always is what I think helped make me successful in my time here.

Finally, I would like to acknowledge my immediate family for their endless support of my dreams and ambitions. None of this would be possible without the support of them, so I owe all my successes to them.

ABSTRACT

Roughness is an important parameter in rock engineering. Sine wave-based simulated wavy profiles were used to investigate systematic changes of amplitude and frequency on roughness indices. Profiles were 1000 mm in length with amplitude ranging from 0-10 mm and frequency ranging from 0-10 Hz. The roughness algorithms used were Root Mean Square (RMS), Energy, Sinuosity, Z2, Mean Absolute Angle (MAA), and Modified Divider a-Value. Roughness indices were visualized as contour plots. Similarities of the shapes and spacing of the contours as well as the magnitude of the roughness indices prompted the pairing of RMS and Energy algorithms, Z2 and MAA algorithms, and Modified Divider a-Value and Sinuosity algorithms.

Equations were developed to relate the paired roughness algorithms. The process for developing the equations began with producing best-fit surfaces of the roughness indices contour plots and assessing their validity using a tolerable percentage difference of 5% between roughness indices and best-fit surface-derived roughness indices. A translation equation was developed using the paired algorithms' roughness indices and a best-fit surface to the translation equation data. The roughness indices of one of the paired algorithms multiplied by the translation factor yielded the computed roughness indices of the other paired algorithm. The computed roughness indices were compared to the roughness indices using a tolerable percentage of 5%. The equation linking Energy and RMS was successful at estimating the true roughness indices 83.3% of the time for a 5% tolerable difference. The equation linking Z2 and MAA was successful at estimating the true roughness indices 73.8% of the time for a 5% tolerable

difference. The equation linking Sinuosity and Modified Divider a-Value was successful at estimating the true roughness indices 86.1% of the time for a 1% tolerable difference.

TABLE OF CONTENTS

LIST OF TABLES

LIST OF FIGURES

LIST OF ABBREVIATIONS

a	Fractal Intercept
D	Fractal Dimension
LVDT	Linear Variable Differential Transformer
MAA	Mean Absolute Angle algorithm
RMS	Root Mean Square algorithm
Z2	Z2 algorithm
MDA	Modified Divider a-Value
CRRA	Cumulative Relative Relief Amplitude
WGA	Weighted Average Gradient
SF	Structure Function
JRC	Joint Roughness Coefficient
JCS	Joint wall Compressive Strength

CHAPTER ONE: INTRODUCTION

1.1 Research Background

Surface roughness is the microtopography of a surface. Microtopography refers to the peaks and valleys of varying heights and lengths on a surface. Surface roughness is of interest in many technical fields, specifically those dealing with chemical processes occurring on surfaces or where there are two contacting surfaces.

The surface roughness of rock joints is an important parameter; the strength, stiffness, and fluid flow properties of a rock mass depend on the surface roughness of rock joints. The shear resistance of rock joints was found to be affected by the joint surface undulations and the friction between the two contact regions (Dong et al., 2022). This friction between contact regions is a function of the roughness, and it was found that the stiffness of rock joints will also increase with the increase of joint roughness (Xuezhen et al., 2022). The roughness along a rock joint can also determine how well fluid can flow through these discontinuities and if the roughness of the rock joint affects that flow. Luo et al. (2016) found that fluid moved easiest through rock joints in high-aperture regions.

Patton (1966) introduced the concept of two different scales of roughness associated with rock joints: waviness and unevenness. Waviness is the large-scale roughness that occurs on a decimeter or meter scale. Unevenness is the small-scale roughness that occurs on a millimeter or centimeter scale. The two roughness components have different contributions to the shear strength of a rock discontinuity (Yang et al., 2001).

Building on Patton's work, Barton (1973) introduced a new rock joint shear strength equation that incorporates a roughness parameter JRC (joint roughness coefficient). Barton and

Choubey (1977) created ten standard profiles used to assess the JRC values. The standard profiles have JRC values that range between zero and twenty in steps of two. A joint surface is visually compared to the standard profiles, and a JRC value is chosen.

Roughness algorithms are mathematical techniques used to quantify the varying microtopography of a profile (2D) or a surface (3D). The algorithms are applied in either the spatial domain or the frequency domain. When assessing the roughness of a profile, the roughness algorithms provide either a single number, termed the roughness index, or in the case of fractal algorithms, two values which are the fractal dimension (D) and the fractal intercept (a).

Since the introduction of the standard JRC profiles, research in quantifying joint roughness has followed two general themes. Researchers have digitized the JRC profiles and quantified them using roughness algorithms. This has resulted in the development of numerous equations where JRC is a function of roughness indices determined through the roughness algorithms. Researchers also began to measure the microtopography of real rock joints and failure surfaces to quantify their roughness using roughness algorithms.

Quantifying the roughness of real rock joints is important for rock engineering design. However, there are two main difficulties with assessing real joint surfaces. Firstly, it is impossible to quantify the roughness of all rock joints in a rock mass, so the full range of microtopographies cannot be assessed. Secondly, the individual contributions of large-scale waviness and small-scale unevenness to roughness indices are still unknown. To overcome these difficulties, this research focuses on systematically determining the roughness indices of simulated wavy roughness as a function of amplitude and frequency to assess the contribution of waviness to roughness. Herein, wavy roughness is defined as the absence of small-scale asperities superimposed on larger-scale surface fluctuations. As such, smoothly undulating profiles will be analyzed in this thesis.

1.2 Research Objective

This study investigates the roughness of simulated large-scale wavy profiles using common roughness algorithms. The simulated wavy profiles will be developed by systematically varying the amplitude and frequency of sine waves. The simulated profiles will be quantified using six common roughness algorithms that have been implemented into MATLAB®. The computed roughness indices will be assessed as a function of amplitude and frequency for each of the roughness algorithms.

1.3 Research Questions

The following research questions are proposed to achieve the objective of this study:

- Is it possible to visualize roughness indices as a function of amplitude and frequency?
- How does systematically changing the amplitude and frequency of a sine wave profile affect the roughness index of a given roughness algorithm?
- Is it possible to establish a comparative relationship between the roughness indices of different algorithms?
- Is it possible to develop equations to relate the roughness indices of roughness algorithms?

1.4 Limitations of the Research

The limitations of this research include the profiles analyzed and the algorithms implemented. The profile limitations include 2-dimensional versus 3-dimensional analyses, amplitude and frequency of the sine waves, the profile's length, and the sine wave's discretization. The algorithm limitations include the choice of algorithms being used and the component of roughness being analyzed.

1.4.1 Profile Limitations

The objective of this research is not to assess the roughness of natural rock surfaces but to systemically assess how changes in amplitude and frequency of a sine wave affect roughness

using roughness indices. Amplitude and frequency values were selected to encompass extreme values associated with rock joints. Amplitude values are ±10 mm from a mean horizontal line. Frequency values range between 0 to 10 Hz.

Once the minimum and maximum values of amplitude and frequency were set, it was necessary to use a step size to systematically vary the two parameters. The step size is 0.5 mm for amplitude and 0.1 Hz for frequency. These small step sizes ensure that a reasonable data set is developed. However, small-scale features may be missed because of the step size that was chosen.

All simulated profiles have a length of 1000 mm. This length was chosen due to large-scale waviness being on the order of decimeters to meters. The JRC profiles developed by Barton and Choubey (1977) have lengths of 10 cm, and it is believed that creating simulated profiles ten times the length of the JRC profiles would be sufficient. However, simulated low-frequency profiles may be underrepresented in the generated datasets because they will not have a repeating pattern within the 1000 mm profile length.

The sine wave profiles are symmetrical. Their symmetry may impact the computed roughness indices. The symmetrical profiles do not accurately represent a real rock profile.

Rock joints are three-dimensional surfaces. This research is focused on assessing the effects of varying amplitude and frequency on two-dimensional profiles. The simulated profiles used in this research are not meant to represent a complex natural rock joint profile or surface.

Prior research has shown there are two components of roughness: large-scale waviness and small-scale unevenness. This research is solely focused on assessing the contribution of waviness to roughness. It has been found that both scales of roughness need to be considered to quantify the roughness of a profile accurately. The definition of waviness for this thesis is the absence of smaller-scale unevenness.

1.4.2 Algorithm Limitations

Numerous algorithms have been used to quantify the roughness of a profile or surface. The algorithms that have been selected for this research are the ones that have been found to be the most popular in recent publications on rock roughness. As a result, not all roughness algorithms will be considered when quantifying the simulated profiles.

1.5 Structure of Thesis

The first chapter provides a brief background to roughness as it relates to the shear strength of rock joints. A short discussion on the history of incorporating roughness into rock joint shear strength and recent research efforts in quantifying roughness is presented. This chapter also includes the research objective, research questions, and limitations of the research.

Chapter Two features a literature review that dives deeper into the subject of roughness in rock joints and the topic of JRC. This chapter covers how roughness is quantified and how roughness can affect the shear strength of a rock joint. Within this chapter, the evolution of the shear strength equation in terms of joint roughness is discussed with the different equations that can be used to determine the shear strength of a rock joint. This chapter then moves on to discuss the different ways that surface roughness can be measured. These methods are called contact and non-contact and are discussed in this chapter. The types of algorithms used within this study will also be discussed, such as what these types of algorithms mean and what they tell us about a joint surface. The chapter then presents a discussion regarding the assessment of the original JRC profiles and the studies of other researchers who used roughness algorithms to characterize these standard profiles. The chapter then concludes by summarizing previous studies in which researchers used simulated profiles or models to characterize rock joint surfaces.

Chapter Three is a discussion of the simulated wavey profiles that will be used in this research. The range of values for amplitude and frequency is discussed, as well as the step size

for amplitude, frequency, and length of the profile. In general, changing the combination of amplitude and frequency will give different values for the roughness index. A wide data set of amplitude and frequency will allow for relationships and correlations to be found regarding specific values of amplitude and frequency, as well as relationships between algorithms. This chapter will feature figures showing these profiles and how they differ with changing parameters.

Chapter Four is dedicated to answering the first research question of how to visualize the roughness indices as a function of amplitude and frequency. Numerous plots are presented, and it focuses on how these plots were created and the software that was used to create them. Visualizing these roughness indices is important because it allows us to see how they can be visualized as a function of amplitude and frequency. Different plots can be used to visualize the roughness indices, and these will be discussed in this section. This section will include the figures of the roughness indices of each used roughness algorithm. This chapter answers the first and second research questions about how it is possible to visualize roughness indices as a function of amplitude and frequency and how systematically changing the amplitude and frequency affects the roughness index.

Chapter Five of this thesis discusses the comparative relationships that were found between the different roughness algorithms. The pairing of the algorithms and why the algorithms were paired are discussed. This chapter answers the third research question of whether it is possible to establish a comparative relationship between the roughness indices of different algorithms.

Chapter Six of this thesis presents the development of equations linking the paired algorithms. In this chapter, best-fit surface equations in terms of amplitude and frequency have been determined for all roughness algorithms. The percentage difference between roughness indices and computed roughness indices was used to assess the goodness of fit. Next, a best-fit surface translation equation was found between paired algorithms which were used to determine

roughness indices from one algorithm from roughness indices from a different algorithm. The percentage difference between actual and computed roughness indices was used to assess how well the linking equations worked. This chapter answers my final research question of if it is possible to develop equations to relate the roughness indices of roughness algorithms.

Chapter Seven is the last chapter of this thesis and presents a summary of the work performed and the results. It also presents a discussion of potential future work.

CHAPTER TWO: LITERATURE REVIEW

Roughness is a fundamental property of surfaces that is important in various scientific fields, including physics, engineering, and biology. The roughness of a surface affects its mechanical, thermal, and electrical properties. In physics, roughness can affect the flow of fluids and heat transfer. This can be seen where roughness induces perturbations in the velocity profile, which affects the surface drag (Kadivar et al., 2021). In engineering, roughness is a vital factor in the design and performance of machines, such as gears and bearings (Benson et al., 2013). In biology, roughness plays a role in cell adhesion and the interaction between biological surfaces (Zareidoost et al., 2012). Overall, the study of roughness is essential for understanding and improving the performance of materials and systems in various technical specialties.

In civil engineering, roughness is important in many applications. For roadways, roughness affects the level of driver comfort and the consumption of fuel (Greene et al., 2013). For bridges, roughness can affect the flow of water and contribute to scouring and erosion (Pagliara and Carnacina, 2010). For water distribution systems, roughness can impact the flow of water and energy loss through the pipes, leading to decreased efficiency and increased pumping costs (Nyende-Byakika, 2017). In geotechnical engineering, roughness refers to the irregularity or deviation from a smooth surface on a soil or rock mass. Roughness is an important factor in geotechnical engineering as it affects the stability of slopes, the behavior of soil and rock masses, and the performance of retaining structures. In slope stability, roughness can increase the shear strength of soil and rock masses, making them more resistant to sliding or failure (Kim et al., 2013). In retaining structures, roughness can affect the stability of retaining walls and the distribution of pressure on the wall due to the increase of friction between the wall and soil.

2.1 Roughness and Shear Strength of Rock Joints

The shear strength (τ) of a rock joint can be expressed in terms of the Mohr-Coulomb failure criterion as:

$$\tau = \sigma_n \tan \phi \qquad \textbf{Equation 2.1}$$

where σ_n is the normal stress acting on the joint surface and ϕ represents the friction angle of the rock joint. In this formulation, the roughness is incorporated into the friction angle term, and the increase in roughness increases the friction angle.

Newland and Alley (1957) introduced a new equation for the estimation of the shear resistance of sands and granular soils:

$$\tau = \sigma_n \tan(\phi_b + i) \qquad \textbf{Equation 2.2}$$

This equation features τ as the maximum shear strength, σ_n as the effective normal stress, ϕ_b as the angle of frictional sliding resistance between particles, and i represents the average angle of deviation of particle displacements from the direction of the applied shear stress.

Patton (1966) observed the equation proposed for sands and granular soils and concluded that this equation could represent irregular joint surfaces but only under low normal stress conditions. Patton proposed a bilinear envelope equation that describes the shear resistance under both high and low normal stress conditions. The Coulomb linear relationship was used to describe the shear strength at high normal stresses because it is assumed to be satisfied due to the irregularities expected to be sheared off. These bilinear envelopes are:

$$\tau = \sigma_n \tan(\phi_b + i) \text{ at low normal stresses} \qquad \textbf{Equation 2.3a}$$

$$\tau = c + \sigma_n \tan \phi \text{ at high normal stresses} \qquad \textbf{Equation 2.3b}$$

In the above equations, the variables represent the same variables as in Equations 2.1 and 2.2. The high normal stress condition equation features the Coulomb parameters of (c) and (ϕ), where c represents the cohesion and ϕ represents the interface friction angle.

Patton (1966) also introduced the concept of two different scales of roughness. He identified large-scale waviness and small-scale unevenness. Waviness appears on a decimeter-to-meter scale, and unevenness appears on a millimeter-to-centimeter scale. These two scales have different contributions to the shear strength of a rock joint. During small displacements, the behavior of the rock joint is primarily controlled by the unevenness of the profile. The waviness of the profile governs the shearing process of the rock joint at higher displacements. Patton found that the large-scale waviness has a larger contribution to the shear strength under natural surfaces due to the small-scale unevenness typically failing under creep or weathering.

Figure 2.1 represents the two scales of roughness that can be seen on a profile. The profile on the top represents the high-frequency, low-amplitude unevenness. The middle profile represents the low-frequency high amplitude waviness. The combination of the two profiles, which is meant to represent a real rock profile, is the third profile. This profile is represented as a thick line because it is a combination of unevenness and waviness. The inset figure shows a magnified view of the combined profile.

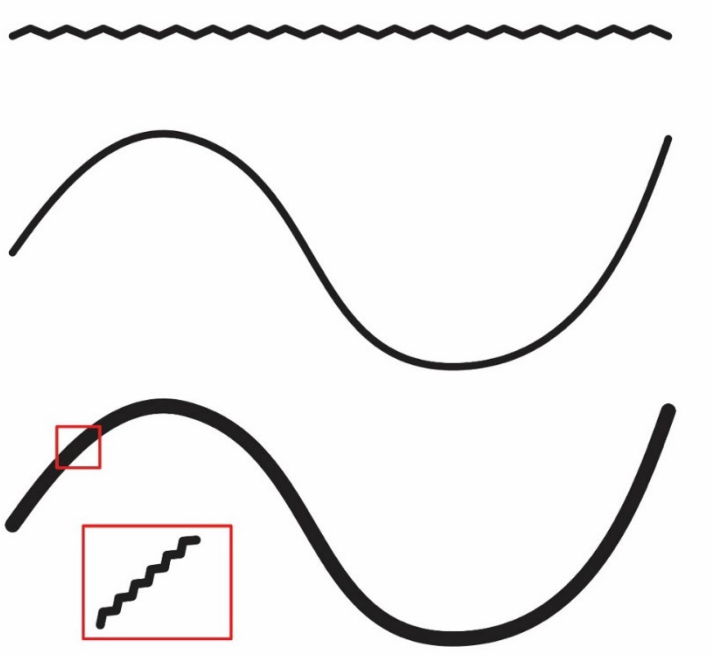

Figure 2.1 Profile showing the locations of the two different scales of roughness.

According to Patton (1966), at low normal stress levels, the unevenness of the profile controls the shearing process. However, as the normal stress acting on the rock joint increases, the unevenness of the rock surface begins to shear off, which causes the waviness of the profile to take over the shearing process. Patton's discovery of the roughness of rock joints affecting the shearing process of a discontinuity led to the incorporation of rock joint roughness into the rock joint shear strength.

Barton (1973) proposed an enhanced frictional portion of the Mohr-Coulomb criterion. This new shear strength equation features only the frictional component because inherent shear strength does not play a role in roughness. The equation, shown in equation 2.4, consists of a joint roughness coefficient (JRC) value, a joint wall compressive strength (JCS) value, and ϕ_b. JCS is the joint wall compressive strength, which is equal to the unconfined compressive strength (often measured using a Schmidt hammer or estimated using the point load test if the joint wall can be sampled). The value of ϕ_b is the friction angle of the surfaces, which incorporates the mineralogical properties of planar rock surfaces, and the JRC is the component that includes the roughness of the discontinuity.

$$\tau = \sigma_n \tan\left[JRC * \log\left(\frac{JCS}{\sigma_n}\right) + \phi_b\right] \qquad \textbf{Equation 2.4}$$

Barton and Choubey (1977) created a visual representation of joint surfaces that can be used to assess the JRC roughness of a given rock profile. These can be considered the first synthetic profiles developed for use in rock engineering. Ten standard profiles were created, shown in Figure 2.2, each with an assigned range of JRC values. The JRC values range from zero to twenty with each profile having a range of two integer values. The ten standard profiles are meant to be used as a guideline to assess the roughness profile of the rock joint of interest. The profiles have a length of 10 centimeters and the horizontal and vertical scales in Figure 2.2 are the same.

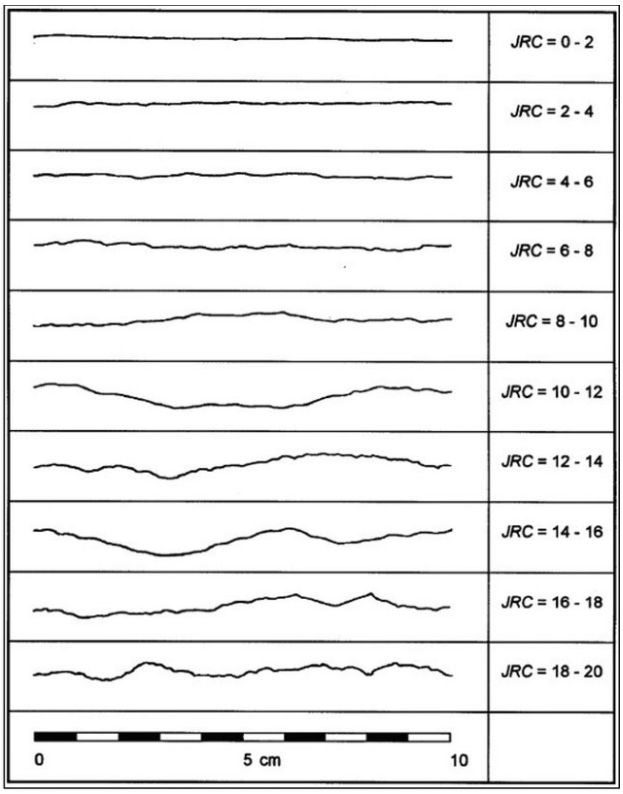

Figure 2.2 JRC Profiles (Barton and Choubey, 1977)

The profile with the smallest JRC profile is relatively planar and is assigned a JRC value of zero to two. This profile lacks both waviness and unevenness. As the JRC values increase, the waviness and unevenness of the profiles increase. It should be noted the increases in waviness and unevenness are not systematically increased from low to high JRC values.

Also included in the Barton and Choubey (1977) study was an updated rock joint shear resistance equation. The updated equation used a new friction angle which is termed as the residual friction angle (ϕ_r). The residual friction angle is used for weathered joints. The improved equation can be found in Equation 2.5. The value of ϕ_r can be estimated based on the ratio between the Schmidt hammer rebound obtained on a saturated weathered joint wall and the rebound obtained on a non-weathered (fresh) dry rock surface.

$$\tau = \sigma_n \tan\left[JRC * \log\left(\frac{JCS}{\sigma_n}\right) + \phi_r\right] \qquad \textbf{Equation 2.5}$$

The development of the JRC profiles and associated roughness values was a tremendous step forward in quantifying roughness and incorporating roughness into the shear strength of rock joints. However, some issues are related to using JRC profiles and values when assessing roughness. Although the JRC profiles cover a wide range of waviness and unevenness, they fail to cover all potential possibilities of surface variations. Using the profiles is very subjective, and professionals with different backgrounds and experiences may select different JRC profiles to represent the same joint surface (Beer et al., 2002). Finally, the range of JRC profiles may not be sufficient to quantify roughness values for real joint surfaces.

2.2 Measuring Microtopography of Surfaces

Many methods have been developed and used to measure microtopography either along a line (profile) or on a surface. Measuring techniques can be divided into two broad categories: contact and non-contact methods. Contact methods require the surface to be physically contacted by a measuring instrument. Examples of these methods include:

- Mechanical Profiling. A rock surface is passed beneath a stationary measuring instrument such as an analog or digital dial gauge or linear variable differential transformer (LVDT), and the change in height is recorded. This technique is used to ensure the tolerance of rock cores for testing (ASTM D4543-19). The stylus for the dial gauge or LVDT will typically have a width larger than the roughness being measured.
- Compass Clinometer. Large-scale roughness can be measured using a compass clinometer. This method only provides an average value for the slope of a rock surface and is not useful for measuring small-scale surface deviations (Fecker and Rengers, 1971).

- Straight Edge. The maximum amplitude usually plays an important role in controlling the shear strength of joints and Barton (1981) proposed a relation between the JRC and the maximum amplitude measured over a sample length. (Milne et al., 1991)
- Contour Gauge Tool. This tool consists of connected pins that can take the shape of a rough surface. This tool is used by carpenters to measure surfaces and make intricate cuts. Like mechanical profiling, the pins have a width larger than the small-scale roughness to be measured (Poropat, 2009).

Contact methods are time-consuming and are often not sufficiently detailed to provide an accurate assessment of roughness. Contact methods may alter fragile surfaces. These methods, however, are less expensive than non-contact methods.

Non-contact methods use imaging technologies to measure the profile without having to physically touch the surface. These methods include:

- Shadow Profilometry. The shadow cast by a ruler reveals the roughness profile across the surface. If the surface is smooth, the edge of the shadow is straight, and if rough, the shadow is irregular. A digital image of the shadow can be obtained and further processed to compute roughness indices (Maerz et al., 1990)
- Photogrammetry. Multiple overlapping images are taken to cover a surface. The images are processed to produce a three-dimensional surface (for example, Kim et al., 2013).
- Laser Scanning. Two- and three-dimensional laser scanning have been used to scan surfaces. The time difference between sending and receiving laser pulses can produce either topographic profiles (2D) or topographic surfaces (3D) (for example, Ge et al., 2015).

Non-contact methods provide many measurements at high resolutions over a short period of time. However, the equipment cost may be prohibitive. Some non-contact measurement systems can only be used in the laboratory.

2.3 Roughness Algorithms

Once a surface microtopography has been measured, the roughness can be quantified using roughness algorithms. These are mathematical techniques used to quantify the varying microtopography of a profile. The algorithms are applied in either the spatial or frequency domain. Roughness algorithms provide either a single number, termed the roughness index, or in the case of fractal algorithms, two values, the fractal dimension (D) and the fractal intercept (a).

There are many different roughness algorithms that have been developed by many different researchers in many different fields of study. This discussion is not meant to be comprehensive, rather it focuses on the different algorithms that are incorporated into this study.

2.3.1 Spatial-Based Algorithms

These algorithms treat the trace of the joint surface as a profile from a contour plot or topographic map. These algorithms are often described and categorized as amplitude algorithms, wavelength algorithms, and slope algorithms.

Amplitude algorithms incorporate changes in height along the profile from a mean reference plane or datum. These algorithms typically assess the vertical distance between the highest peak of the profile and the lowest valley, the vertical distance between the highest peak and the centerline or mean reference plane of the profile, or the average distance between the 5 highest peaks and the five lowest valleys or of all peaks to valleys. Using these algorithms, the roughness index will increase with changes in the amplitude of the profile. Examples of

amplitude-based algorithms include the Root Mean Square (RMS) algorithm (as presented in McCarroll and Nesje, 1996) and the Energy algorithm (as presented in Brown et al., 2016).

Wavelength algorithms incorporate a measurement of the distance between peaks. These algorithms measure the average spacing between each of the adjacent peaks, the number of peaks per unit length of the profile, and the proportion of the length of the profile that has an amplitude that is positive above a preselected vertical distance from the centerline. Using these algorithms, the roughness index will increase with the frequency of peak values with a trace. An example of a wavelength-based algorithm is the Number of Turning Points algorithm (as presented in McCarroll and Nesje, 1996).

Slope algorithms incorporate a measure of the average slope within a profile. Typical measurements include finding the root mean square of the first derivative of the asperity heights, determining the root mean square of the second derivative of the asperity heights, and determining the true length of a profile to its projected length in the joint surface. Examples of slope-based algorithms include Z2 (as presented in Tse and Cruden, 1979), Sinuosity (as shown in Saleh, 1993 and McCarroll and Nesje, 1996), and Mean Absolute Angle (MAA) (as presented in Parsons, 1988). The measurements incorporated into these algorithms indicate that neither amplitude nor frequency alone drastically affect the roughness index. These algorithms portray the effects of both amplitude and frequency.

2.3.2 Fractal Algorithms

In general, a fractal is an infinitely complex mathematical shape that repeats across an infinite range of scales. There are two different categories of fractals: self-affine and self-similar. Self-similar fractals are statistically equivalent when scaled equally on both axes. If a self-similar fractal were placed underneath a magnifying glass with infinite magnification, the fractal would be the same no matter the level of magnification. Self-affine fractals must be scaled differently in perpendicular directions to maintain statistical similarity. For the same scenario with the fractals

being underneath a magnifying glass, if you magnified a self-affine fractal, the shape would always change depending on the level of magnification (Mandelbrot, 1983).

Fractal algorithms provide two measurements: the fractal dimension (D) and the fractal intercept (a). The fractal dimension is a non-integer value typically less than the dimension of space in which that profile exists (Goehring and Morris, 2015). For example, a profile is two-dimensional, but the fractal dimension of the profile would be less than two. The fractal dimension represents how well an irregularly shaped object fills the space that it occupies (Huang et al., 1992). It also measures the relative amounts of roughness detail occurring over a range of measurements (Vuopio and Pöllä, 1997). The fractal dimension measures the small scale of roughness or unevenness of the profile.

The fractal intercept is a measurement that indicates the degree of vertical topographic variations from a mean reference line (Klinkenberg and Goodchild, 1992). The fractal intercept is a measure of the large-scale roughness or waviness. There is some debate on whether natural fractured surfaces are self-similar or self-affine. Many researchers, including Benoit Mandelbrot (the father of fractal mathematics), claim that fractured surfaces are self-affine.

2.4 Application of Roughness Algorithms and Simulated Profiles

There is a rich literature of the use of roughness algorithms and simulated profiles in rock mechanics and rock engineering research. For this research, the relevant background is applying roughness algorithms and using synthetic profiles. This section presents example studies of assessing simulated profiles using roughness algorithms and simulated profiles.

2.4.1 Assessing Simulated Profiles Using Roughness Algorithms

Once the JRC profiles, often considered to be the first simulated profiles, were published, researchers began digitizing the profiles, assessing the profiles using roughness algorithms, and developing relationships between roughness indices and JRC values. The first of these studies was by Tse and Cruden (1979), who used roughness algorithms that had been used to describe the

finish on milled surfaces. They found a strong correlation between JRC and two roughness parameters Z2 and Structural Function (SF).

Li and Zhang (2015) conducted an exhaustive literature review of previous studies correlating roughness parameters to the JRC coefficients. They found forty-seven different relationships between JRC and roughness indices. Using 112 real rock profiles found in the literature, they derived new relationships between JRC and roughness indices. When deriving new relationships between JRC and other roughness indices, it was found that Z2 and the standard deviation of the angle (σ_i) roughness algorithms were the best in terms of the correlation coefficient, but it was recommended that R_z (maximum height of the profile) and λ (ultimate slope of the profile) should be used within engineering practice due to their easy and convenient determination.

McGough et al. (2015) digitized the ten standard JRC profiles. They found the roughness algorithms Z2 and Mean Absolute Angle (MAA) had the highest degree of linearity when their roughness indices were plotted against JRC values. The roughness algorithms' Standard Deviation and Signal Energy were insensitive to sampling interval when digitizing the JRC profiles. They had a low degree of linearity when their roughness indices were plotted against JRC values.

By assessing the JRC profiles, twelve synthetic profiles, and a numerical shear model, Yuan et al. (2021) developed two dimensionless indexes to represent the morphology characteristics of a two-dimensional joint profile. Typically, roughness indices such as Z2 and structure function (SF) are used to characterize a joint profile. Still, these parameters only consider geometric features without considering the mechanical properties of joint shear. The two new parameters are the cumulative relative relief amplitude (CRRA) and weighted average gradient (WAG), which reflect rock joints' climb and friction effects during the shearing process. They found the new parameters were sensitive to sampling intervals but insensitive to scaling.

CRRA and WGA can accurately assess the JRC of a rock joint used for calculating peak shear strength based on Barton's shear strength equation.

Ankah et al. (2021) digitized the JRC profiles at 0.5 mm sampling intervals and used seven different roughness algorithms to develop equations relating single algorithms to JRC values. The algorithms that were incorporated into this study were average asperity angle A_i, mean positive inclination angle of the profile θ_{p+}, mean negative inclination angle of the profile θ_{p-}, the standard deviation of the inclination angle of the profile SD, root mean square of the slope of the function Z2, structure function SF, and the maximum apparent dip angle in the shear direction $\theta^*_{Max}/[C+1]_{2D}$). Their results showed high values of correlation coefficients for JRC as a function of θ_{p+}, θ_{p-}, A_i, and SF at the 0.5 mm sampling interval.

2.4.2 Use of Simulated Profiles

Quantifying the roughness of real rock profiles can be very difficult due to the variations of microtopography. One problem with using JRC profiles is that a natural rock profile may not be represented in the standard JRC profiles. This limitation can be overcome by producing and assessing simulated profiles. The studies summarized below show the variety of investigations conducted using simulated profiles.

Rasouli and Harrisson (2010) used Riemannian statistics to evaluate the roughness of profiles. In their study, they incorporated symmetric sawtooth profiles, asymmetric sawtooth profiles, sinusoidal profiles, superimposed sinusoidal profiles, JRC profiles, and natural rock profiles. The authors report the Riemannian dispersion parameter (D_{R1}) can be linked to the shear strength of a profile.

Asadi et al. (2012) extended the work of Rasouli and Harrison (2010) by incorporating the synthetic profiles into the two-dimensional discrete element method software Particle Flow

Code (PFC2D) to assess their shearing behavior. Part of their work included generating random profiles with different D_{R1} values.

Stigsson and Ivars (2018) used the inverse of the fast Fourier transform (IFT) of the power spectrum to generate random fractal-based self-affine two-dimensional synthetic traces. They incorporated 1024 traces in their study to ensure they captured a stable mean and variance of the fractal parameters of the Hurst exponent and asperity measure used to generate the profiles. They used the fractal parameters to develop a model which infers the Joint Roughness Coefficient from the fractal parameters of a natural two-dimensional fracture surface.

Sadaat and Taheri (2020) used synthetic and natural rock joints to investigate shear behavior under constant normal stress conditions using a smooth-joint model in Particle Flow Code 2D. They noted that the influence of surface roughness is only sometimes incorporated into shear behavior studies. The synthetic profiles incorporated into their research included a symmetric saw-tooth pattern with asperity angles of 20 and 30 degrees.

Guo et al. (2022) used both prepared rock surfaces and synthetic profiles to quantify roughness using the power spectral density method and conventional roughness algorithms (RMS, Z2, SF, R_p, $\theta^*_{max}/(C+1)$, and SD). Natural rock surfaces were systematically ground, polished, and sheared to provide mesoscale roughness (polished and ground surfaces) and macro-scale roughness (sheared surface). Intermediate-scale roughness synthetic profiles were produced following the procedure outlined in Candela et al. (2009). The synthetic profiles were self-affine fractal surfaces. The conventional roughness algorithms were used to assess the surface roughness, and the roughness indices were normalized for their discussion. The normalized roughness indices for the polished (smooth) to ground (rough) surfaces showed the same trend; they very gradually increased with increasing roughness. The roughness indices for the sheared surfaces did not exhibit similar trends; only SD, Z2, and $\theta^*_{max}/(C+1)$ showed indicated

significant difference in surface roughness. All algorithms except RP showed the same normalized trends for the synthetic self-affine surfaces.

2.5 Chapter Summary

The roughness of rock surfaces is the irregularity of the surface microtopography. Roughness is an essential parameter in rock engineering because it is associated with the frictional resistance between two potentially sliding rock blocks. The effect of roughness has been incorporated into the Mohr-Coulomb failure criterion by adding a scalar value i to the angle of friction value ϕ. The value of i represents the average angle of deviation of particle displacements from the direction of the applied shear stress. Barton and Choubey's Joint Roughness Coefficient (JRC) value has also been directly incorporated into shear strength equations.

Microtopography can be measured in the field or laboratory using contact or non-contact methods along a line (profile) or on a plane. Contact methods are inexpensive but time-consuming because a physical connection must be made between a measuring device and a rock surface. Non-contact methods, as the name suggests, allow you to take measurements without making contact, but they often require expensive equipment.

Once the microtopography is measured, the roughness can be quantified. The quantification is made by either comparing the microtopography to the standard JRC profiles or applying roughness algorithms. There are many roughness algorithms, but the most common are spatially based, and fractal algorithms. Spatially based algorithms either incorporate changes in heights along a profile from a datum, include a measurement of the distance between peaks, or a measure of the average slope within a profile. Fractal-based algorithms either measure the amount of space in which a profile occupies or the amount of variation from a mean reference line.

Roughness algorithms and simulated profiles are often used in rock mechanics and engineering research. The JRC profiles have been digitized and quantified many times to develop relationships between JRC and roughness indices. New roughness algorithms have also been developed based on the JRC profiles. Synthetic profiles have been created based on JRC profiles or natural rock profiles. The synthetic profiles have been assessed using roughness algorithms or as part of computer simulations to determine shear behavior and strength.

The literature review has revealed a noticeable gap in the roughness algorithm–simulated profile literature. A study has not investigated how roughness indices change with systemic variations of amplitudes and frequencies of simulated rough surface profiles. Simulated profiles and not natural rock profiles are preferable because it allows for any potential combination of amplitude and frequency to be used. The systematic Simulated profiles also allow for combinations of low-frequency high amplitude and high-frequency low amplitude which can show the two different scales of roughness and the ability to assess the roughness indices across various scales.

CHAPTER THREE: SIMULATED WAVY PROFILES AND ROUGHNESS ALGORITHMS

Previous research has shown that rock joint profiles can be represented by a simple superposition of sine and cosine waves (Yang et al., 2010). In this thesis, sine waves are used to produce simulated wavy profiles. Sine waves are used because it is easy to manipulate both amplitude and frequency to create a variety of wavy simulated profiles. Waviness is defined as the absence of small-scale asperities superimposed on larger-scale surface fluctuations. Smoothly undulating profiles are produced. Five spatial-based algorithms and one fractal-based algorithm are applied to the simulated profiles to compute roughness indices and fractal parameters as a function of amplitude and frequency. This chapter presents the variables and associated variable ranges to create the simulated profiles, examples of simulated profiles, and a description of the roughness algorithms used to compute the roughness indices.

3.1 Sine Wave Equation

The basic sine wave equation is shown in Equation 3.1,

$$f(x) = a * \sin\big(b(x + c)\big) + d \qquad \textbf{Equation 3.1}$$

The equation incorporates four variables, amplitude (a), frequency (b), and translation factors (c) and (d) along the length of the profile (x). The translation factors were not incorporated into this thesis so that all profiles begin at the origin and the profile was symmetric about the x-axis or mean datum plane. The amplitude and frequency were systematically changed to develop a full suite of profiles, as described below.

3.2 Development of Simulated Wavy Profiles

The simulated wavy profiles, termed profiles, are created using a predetermined set of parameters. These parameters included profile length, length step size, amplitude step size, and frequency step size. All the profiles had a length of 1000 mm. This length was chosen because large-scale roughness (waviness) occurs on a decimeter-to-meter scale.

The length step size, which is the horizontal distance between adjacent points on the profile, was 0.05 mm. A small step size was chosen because of previous work, including Tatone and Graselli (2013), Li and Zhang (2015), and Brown et. al (2016), that showed roughness quantification is sensitive to the sampling frequency of the profile. Tatone and Graselli (2013) and Brown et al. (2016) found that higher sampling frequencies produced higher roughness indices. A step size of 0.05 mm is used because it is on the high end of the sampling frequency for industrial laser scanners used in rock mechanics.

The amplitude range for the profiles was ±10 mm from the mean datum plane. Profiles were systematically produced with an amplitude step size of 0.5 mm. A maximum height difference of ±10 mm along a rock joint should encompass extreme values of topographic variation.

The frequency range for the profiles was 0 to 10 Hz. Profiles were systematically produced with a frequency step size of 0.1 Hz. The frequency step size was chosen to be less than the amplitude step size because it is believed that the frequency will have a greater impact on waviness roughness. The profile parameters, the range of values, and the step sizes used can be found in Table 3.1. The profiles were created by incorporating the sine wave equation, excluding the translation factors, in Microsoft Excel. Separate spreadsheets were created for each amplitude. Within each amplitude spreadsheet, the frequencies were systematically varied. A total of 2,100 simulated profiles were created.

Table 3.1 Simulated Profile Parameters and Values

Profile Parameter	Range of Values	Step Size
Amplitude	0-10 mm	0.5 mm
Frequency	0-10 Hz	0.1 Hz
Length of Profile	1000 mm	N/A
Distance between Points on Simulated Profile	N/A	0.05 mm

3.3 Visual Representation of Simulated Profiles

All the profiles follow the same general trend of a sine wave, but each of the profiles has a different amplitude and frequency. The amplitude affects the wave height from the mean datum surface (x-axis). The frequency affects the number of peaks along the profile. Figures 3.1 and 3.2 are example profiles showing key characteristics.

Figure 3.1 contains the simulated profiles for the baseline case and the extreme case. The baseline case is a horizontal profile with no large-scale roughness or waviness. The extreme case is a profile with an amplitude of 10 mm and a frequency of 10 Hz. The 10 mm amplitude means the peak-to-trough vertical distance is 20 mm. A frequency of 10 Hz results in twenty-eight peaks in the 1000 mm profile length.

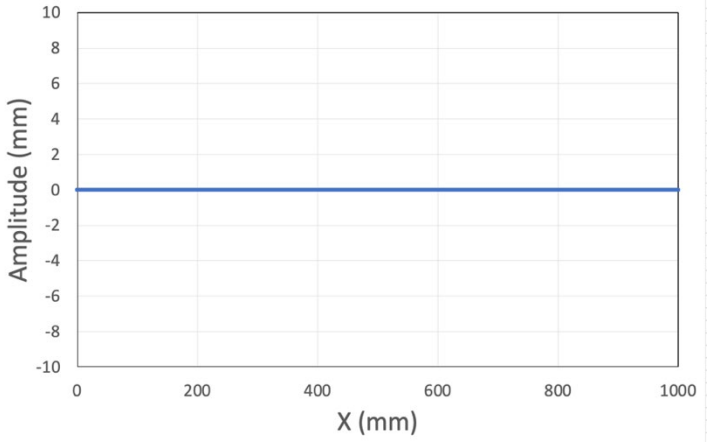

Figure 3.1a: Baseline profile

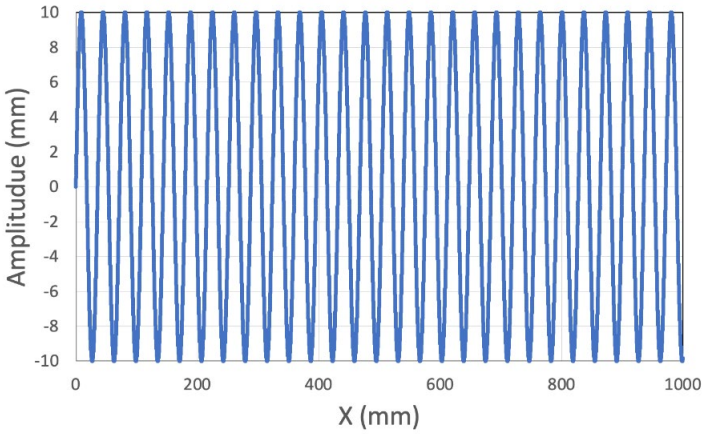

Figure 3.1b: Extreme profile

Figure 3.1 Baseline and Extreme Profiles

Figure 3.2 presents select examples of profiles at different frequencies and a constant amplitude of 5 mm. They are presented in this form because it is often more intuitive to visualize amplitudes rather than frequency. The simulated profiles feature frequencies of 0.1, 0.4, 1.3, and 5 Hz.

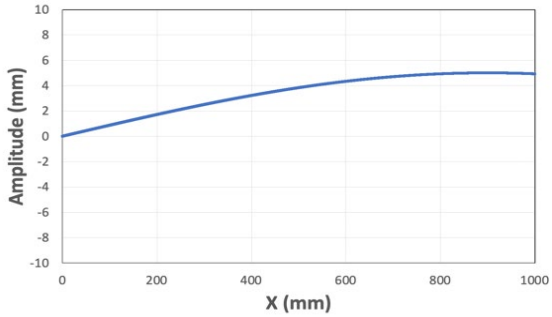

Figure 3.2a: Frequency = 0.1 Hz

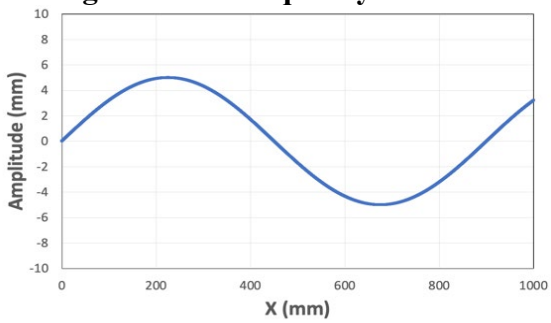

Figure 3.2b: Frequency = 0.4 Hz

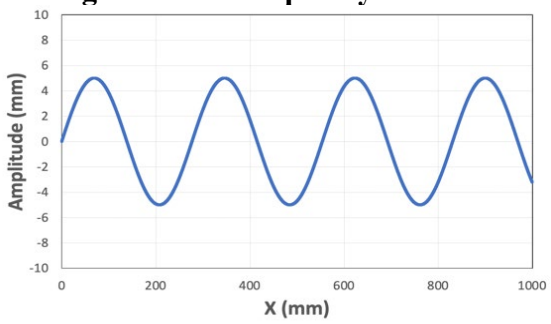

Figure 3.2c: Frequency = 1.3 Hz

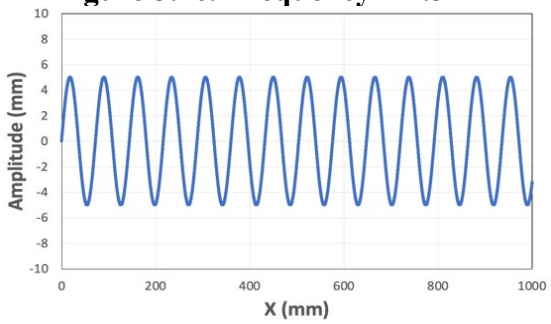

Figure 3.2d: Frequency = 5 Hz

Figure 3.2 Examples of Profiles at Varying Frequencies with a constant Amplitude of 5 mm

At the lowest frequency, 0.1 Hz, the simulated surface is a gentle ramp starting at the beginning of the trace to the end of the trace. At this frequency, one quarter of a sine wave is present. It is expected this low frequency profile will yield a lower roughness index when compared to the other profiles. The simulated profile with a frequency of 0.4 Hz shows a complete wave. Typically, it would be expected that a frequency of 1 Hz, would produce a single complete sine wave. One Hertz is one cycle per second. The methodology used to create the simulated profiles used a length scale, not time scale, on the x-axis. The simulated profile with a frequency of 1.3 Hz shows approximately three and a half sine waves within the 1000 mm profile. The simulated profile with a frequency of 5 Hz is half the maximum frequency. This simulated surface has fourteen positive peaks and fourteen negative peaks within the 1000 mm length.

3.4 Roughness Algorithms

There are numerous roughness algorithms that have been developed and used to quantify the roughness of rock surfaces. This thesis uses six common roughness algorithms to quantify the roughness of the synthetic profiles. The algorithms featured in this chapter are Root Mean Square (RMS), Energy, Sinuosity, Z2, Mean Absolute Angle (MAA), and the fractal algorithm Modified Divider. These roughness algorithms will be used to determine the roughness indices at different combinations of amplitude and frequency.

3.4.1 Root Mean Square (RMS) Roughness Algorithm

The Root Mean Square (RMS) algorithm measures the average deviation from the centerline. If a profile is horizontal (the baseline case), the roughness index for RMS is zero (Brown et al., 2016). The equation for the Root Mean Square algorithms is:

$$R_{RMS} = \sqrt{\frac{1}{N}\sum_{i}^{N}(x_i - \overline{x})^2} \qquad \textbf{Equation 3.2}$$

3.4.2 Energy Roughness Algorithm

The Energy algorithm, which is also known as signal energy, is a parameter that is often used in electrical engineering. It relates the signal energy to the integral of the square of the Fourier transform of the signal (McGough et al., 2015). It is calculated by finding the sum of the squared points and dividing them by the length of the profile. The energy value for a horizontal profile is zero (Brown et al., 2016). The equation for the Energy algorithm is:

$$R_E = \frac{1}{L}\sum_{i=1}^{N}(x_i - \overline{x})^2 \qquad \textbf{Equation 3.3}$$

3.4.3 Z2 Roughness Algorithm

Z2 is calculated by finding the root mean square of the first derivative and describes the magnitude of the incremental rate of change of a profile. The Z2 roughness index for a horizontal line (baseline case) is zero (Brown et al., 2016). The equation for the Z2 algorithm is:

$$R_{Z2} = \left[\frac{1}{L}\sum_{i=1}^{N-1}\frac{(y_{i+1}-y_i)^2}{(x_{i+1}-x_i)}\right]^{1/2} \qquad \textbf{Equation 3.4}$$

3.4.4 Sinuosity Roughness Algorithm

Sinuosity is calculated by dividing the arclength of the profile by the horizontal distance between the beginning and end of the profile. The sinuosity of a horizontal profile results in a roughness index of one (Brown et al., 2016). The equation for the Sinuosity algorithm is:

$$R_S = \frac{1}{L}\sum_{i}^{N-1}\sqrt{(y_{i+1} - y_i)^2 + (x_{i+1} - x_i)^2} \qquad \textbf{Equation 3.5}$$

3.4.5 Mean Absolute Angle (MAA) Roughness Algorithm

Mean Absolute Angle (MAA) measures the average angular difference between adjacent points on a profile. The MAA roughness index for a horizontal profile is zero (Brown et al., 2016). The equation for the MAA algorithm is:

$$R_{MAA} = \frac{1}{N}\sum_{i}^{N-1} \tan^{-1} \left|\frac{y_{i+1}-y_1}{x_{i+1}-x_1}\right| \quad \textbf{Equation 3.6}$$

3.4.6 Modified Divider Fractal Roughness Algorithm

The Modified Divider Method is a fractal algorithm that implements a horizontal divider span along a given profile (Brown, 1987). Each increment along the profile is defined as r_1, r_2, r_3, etc. The incremental lengths along the profile from x_1 to x_{i+1} can be summed to obtain the true length of the profile. The length is summed to obtain the estimated length L where L is proportional to r^{1-D}, where D is the fractal dimension. To determine the fractal dimension, a regression analysis is performed on a plot with the log of the total length on the x-axis and the log of the divider span on the y-axis. The fractal dimension can be calculated by $D = 1 - \beta$ where β is the slope of the linear regression line (Develi and Babadagli, 1998). The relationships between L, D, and r and a can be seen below in Equation 3.7 and 3.8.

$$L = ar^{1-D} \quad \textbf{Equation 3.7}$$

$$\log L = \log a + (1 - D)\log r \quad \textbf{Equation 3.7}$$

The gradient of the line created by 1-D is shown in Equation 3.7 and this is the equation that can be used to determine the fractal intercept (a) (Jang et. al, 2014). Although the modified divider fractal algorithm provides two parameters, this thesis will only use the fractal intercept. Cox and Wang (1993) found the fractal dimension best characterizes the unevenness of a profile whereas the fractal intercept best characterizes the waviness of a profile. The fractal dimension for a horizontal line or the baseline case is the minimum roughness index of 2.998.

3.5 Chapter Summary

Twenty-one hundred wavy sine wave-based synthetic profiles were generated by systematically varying amplitude and frequency. Waviness is defined as the absence of small-scale asperities superimposed on larger-scale surface fluctuations. The profiles were smoothly

undulating. All the profiles are 1000 mm in length. Each profile consists of 20000 points, which corresponds to a horizontal spacing of 0.05 mm. The profiles range between a horizontal profile (base line case) to a profile having an amplitude of 10 mm and a frequency of 10 Hz (extreme case). To develop the profiles, the amplitude and frequency were systematically varied using increments of 0.5 mm and 0.1 Hz, respectively.

Six common roughness algorithms have been chosen to be used in this thesis. There are five spatial roughness algorithms (Root Mean Square, Energy, Z2, Sinuosity, and Mean Absolute Angle) and one fractal algorithm (Modified Divider). The spatial roughness algorithms provide a single value, termed the roughness index, to quantify roughness. The fractal algorithm provides two measures, the fractal dimension and the fractal intercept to quantify roughness. Only the fractal intercept will be used because it is associated with waviness. The spatial algorithms yield a roughness index of either zero or one for the baseline profile.

CHAPTER FOUR: VISUALIZATION OF ROUGHNESS INDICES AND EFFECTS OF VARYING AMPLITUDE AND FREQUENCY

This chapter answers the research questions "Is it possible to visualize roughness indices as a function of amplitude and frequency?" and "How does systematically changing the amplitude and frequency of a sine wave profile affect the roughness index provided by a given roughness algorithm?". Presented in this chapter are contour plots of roughness indices as a function of amplitude and frequency and associated discussions of observations from the contour plots. These discussions include the magnitude of roughness indices, the sensitivity of roughness indices, and the locations, in terms of amplitude and frequency, of the minimum and maximum roughness indices. From the shapes of the roughness indices contour plots, algorithms are grouped for further analyses.

4.1 Visualization of Roughness Indices

Roughness algorithms were programmed into MATLAB® and roughness indices and fractal intercepts were computed for all 2100 simulated profiles. Contour plots of amplitude (Y-axis), frequency (X-axis), and roughness index or fractal intercept (Z-axis) were produced to visualize the results. Contour plots were generated using the commercially available program Surfer by Golden Software.

The contour plots were produced using the geostatistical method Kriging, which is commonly used to predict values of a variable at locations where the variable has not been measured. The method incorporates the spatial variation as represented in a variogram or covariance function. Using ordinary Kriging, no other information than the measured variable plus their locations is needed (McKillup and Dyar, 2014; Oliver and Webster, 2015).

4.2 Roughness Indices and Fractal Intercept as a Function of Amplitude and Frequency

Roughness indices or the fractal intercept value computed using the six roughness algorithms are visualized as a function of amplitude and frequency by using contour plots with the roughness index or fractal intercept as the z-variable. Contour plots are a convenient method to assess changes in roughness indices as amplitude and frequency of the profiles are systematically varied.

4.2.1 Observations from RMS Roughness Indices

The contour plot of roughness indices as a function of amplitude and frequency for the Root Mean Square (RMS) algorithm is shown in Figure 4.1. The minimum roughness index within the bounds of the study is 0.15 at an amplitude of 0.5 mm and a frequency of 0.1 Hz. The maximum roughness index is 7.29 at an amplitude of 10 mm and a frequency of 0.3 Hz.

There are two apparent features present in the plot. On the left-hand side of the plot there are closely spaced contours representing a rapid increase in roughness indices at all amplitudes up to a frequency of approximately 0.5 Hz. The second feature of interest appears after a frequency of 0.5 Hz. Here the contour lines are horizontal indicating at a constant amplitude and increasing frequency, there is no change in the roughness index.

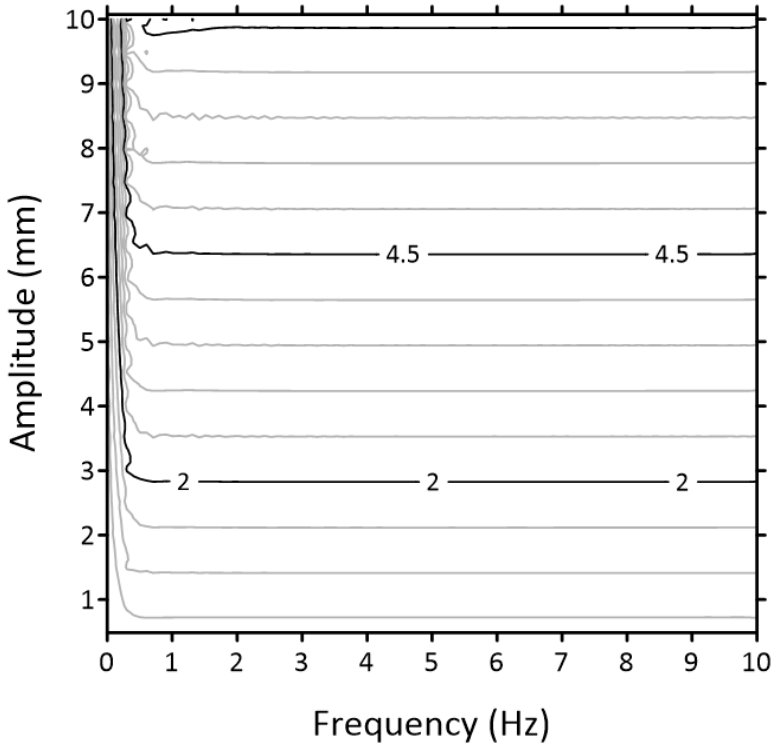

Figure 4.1 RMS Roughness Indices as a Function of Amplitude and Frequency

Since the data are plotted as a contour plot, it is a 2-dimensional representation of 3-dimensional data. To help better visualize the data, a 3D surface plot was created and shown in Figure 4.2. This plot has the same x- and y-axes as the contour plot but the roughness indices are plotted as a surface. It is easy to see the rapid increase of roughness indices as low frequencies and the constant roughness indices at constant amplitudes and increasing frequencies. There is also a linear increase in roughness indices with increasing amplitudes at constant frequencies.

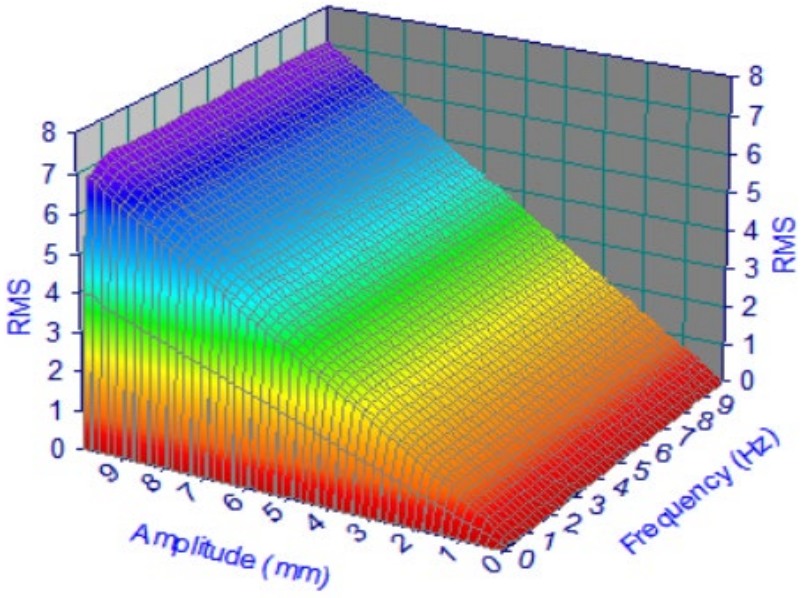

Figure 4.2 3D Visualization of RMS Roughness Indices as a Function of Amplitude and Frequency

To further investigate the effects of amplitude and frequency on roughness indices, cross-sections were taken at a constant amplitude of 5 mm and a constant frequency of 5 Hz, as shown in Figure 4.3. The amplitude and frequency were chosen because they represent the midpoint of the amplitude and frequency ranges. These cross-sections provide profile views of the variation of roughness index as a function of amplitude at a constant frequency and the variation of roughness index as a function of frequency at a constant amplitude.

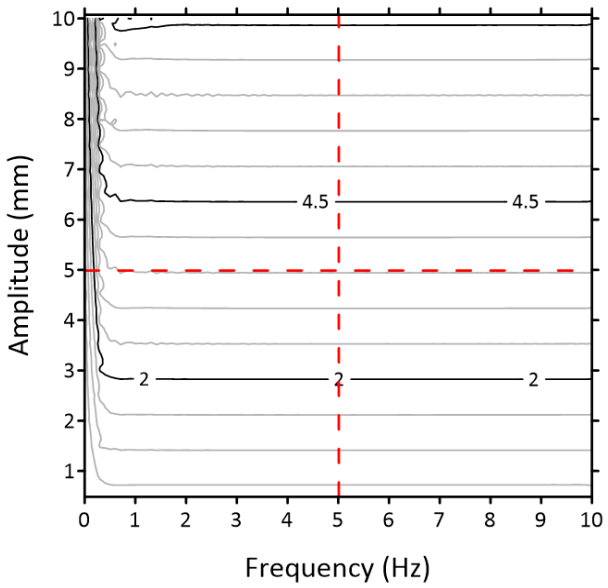

Figure 4.3a: Location of Cross-Sections for RMS Algorithm

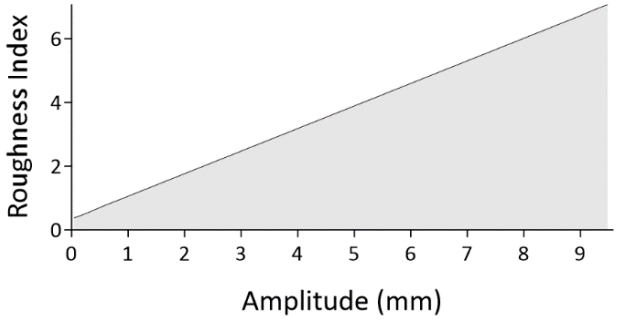

Figure 4.3b: RMS Roughness Indices Profile at Constant 5 Hz Frequency

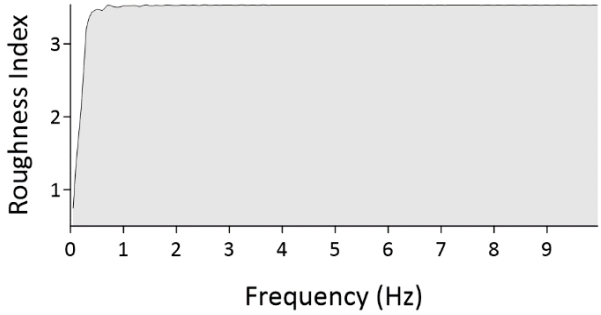

Figure 4.3c: RMS Roughness Indices Profile at Constant 5 mm Amplitude
Figure 4.3 Cross-Sections from the Root Mean Square Plot

The cross-section plot of the constant frequency, Figure 4.3b, clearly shows the roughness index increases linearly with amplitude for a constant frequency. This linear trend is evident for frequencies between approximately 0.5 Hz to 10 Hz.

The cross-section plot of the constant amplitude, Figure 4.3c, clearly shows a rapid initial rise in the roughness index, followed by a series of perturbations, and an eventual leveling off of the roughness index to a constant value. There is a similar trend for profiles at other constant amplitudes.

A closer inspection of the contour plots (Figure 4.1 or 4.3a) or the three-dimension plot (Figure 4.2) shows that in the frequency range of 0 to approximately 0.3 Hz, the contour spacing is greater at low amplitudes and becomes progressively smaller at higher amplitudes. This indicates the slope of the rapid rise portion of the plot is increasing with increasing amplitude. Figure 4.4 shows the roughness indices at amplitudes of 0.5 mm, 5 mm, and 10 mm at frequencies between 0 Hz and 0.3 Hz. Although the slope is not linear between roughness indices and frequency, the average slope is increasing as amplitude increases.

Figure 4.3c also contains an interesting feature. There is a steep rise in roughness indices, followed by a series of perturbations, and then a constant value of roughness indices for a constant amplitude. Figure 4.5 presents the roughness indices at constant amplitudes of 0.5 mm, 5 mm, and 10 mm for a frequency range of 0.3 Hz to 10 Hz. The frequencies are plotted on a logarithmic scale to accentuate the trends of the roughness indices. At low amplitudes, there are very small or nonexistent perturbations. At higher amplitudes perturbations increase in size and the length of the perturbations increase with increasing amplitude. For example, at an amplitude of 5 mm the perturbations end at a frequency of approximately 1.6 Hz and at an amplitude of 10 mm the perturbations end at a frequency of approximately 2.5 Hz.

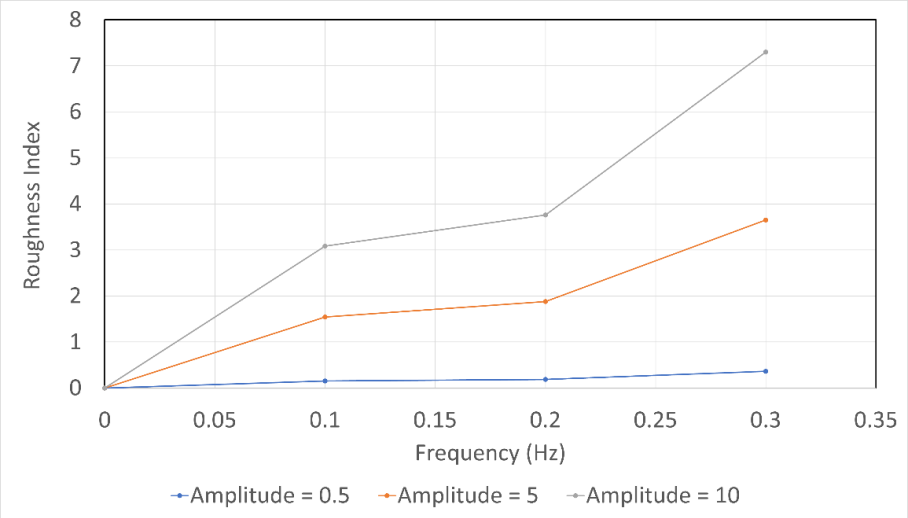

Figure 4.4 Change in Roughness Index with Increasing Frequency at Constant Amplitudes.

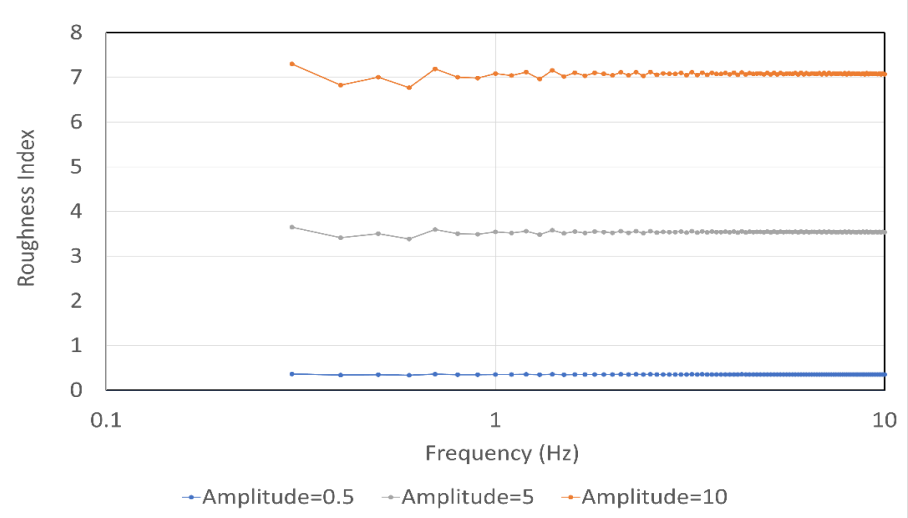

Figure 4.5 Perturbations of Roughness Indices with Increasing Frequency at Constant Amplitudes

4.2.2 Observations from Energy Roughness Indices

The contour plot of the roughness indices as a function of amplitude and frequency for the Energy algorithm is shown in Figure 4.6. This plot is very similar to the RMS plot (Figure 4.1). The maximum roughness index is 54.708 at an amplitude of 10 mm and a frequency of 0.1 Hz. The minimum roughness index, disregarding the baseline case, is 0.1139 at an amplitude of 0.5 mm and a frequency of 0.2 Hz.

In Figure 4.6, at low frequencies there is a rapid increase in roughness indices until a frequency of approximately 0.3 Hz. After 0.3 Hz, the roughness indices are relatively constant at a constant amplitude and increasing frequencies.

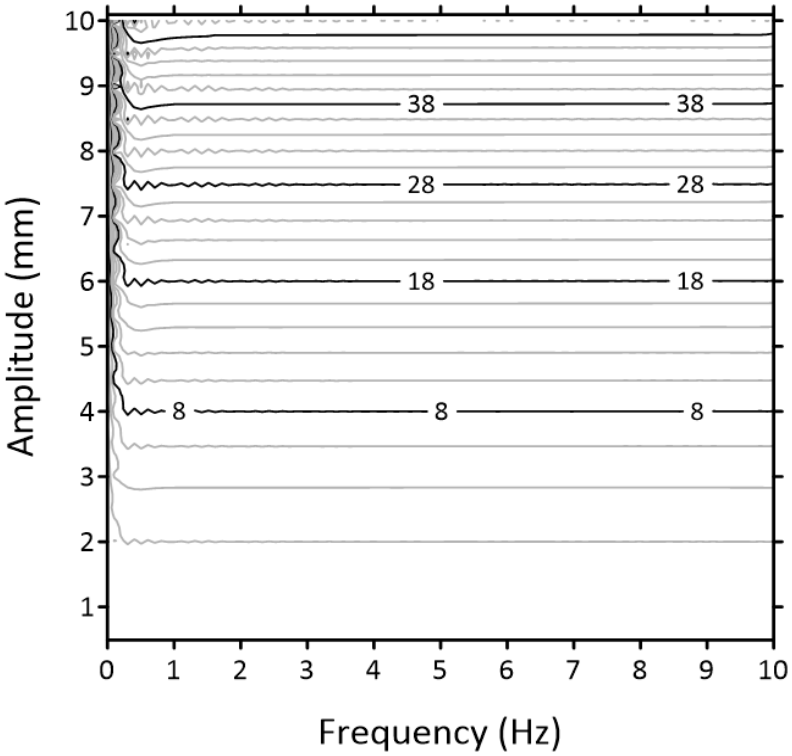

Figure 4.6 Energy Roughness Indices as a Function of Amplitude and Frequency

Due to the data being plotted as a contour plot, it is a 2-dimensional representation of 3-dimensional data. To provide a supplemental visualization of the data, a 3D surface plot was created and shown in Figure 4.7. This plot features the same x- and y-axes as the contour plot but the roughness indices are plotted as a surface. It is easy to see the rapid increase of roughness indices at low frequencies and the constant roughness indices at constant amplitudes and increasing frequencies. There is also a non-linear increase in roughness indices with increasing amplitudes at constant frequencies.

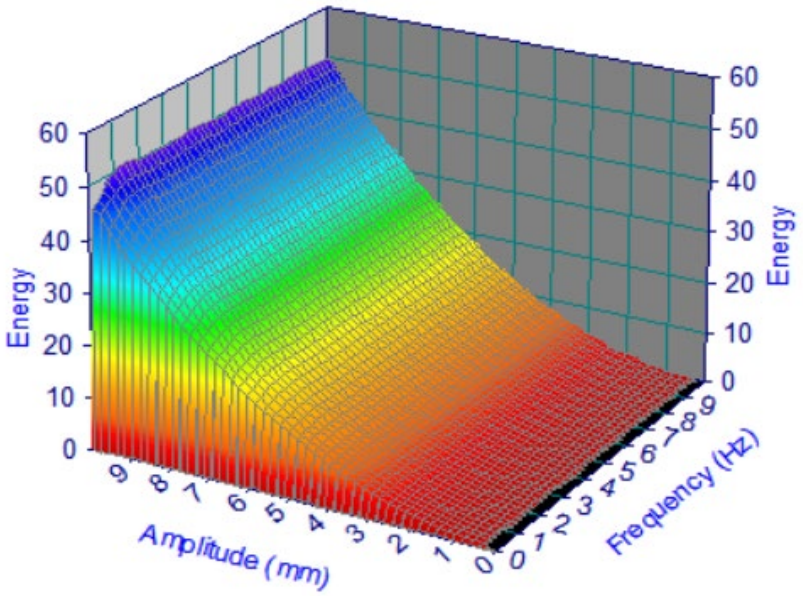

Figure 4.7 3D Visualization of Energy Roughness Indices as a Function of Amplitude and Frequency

Similar to the plots provided in Figure 4.3, cross-sections were taken at the midpoint of the amplitude and frequency ranges (5 mm and 5 Hz) and are shown in Figure 4.8. These cross-sections provide profile views of the variation of roughness index as a function of amplitude at a constant frequency and the variation of roughness index as a function of frequency at a constant amplitude. The cross-sections and their locations are shown in Figure 4.8.

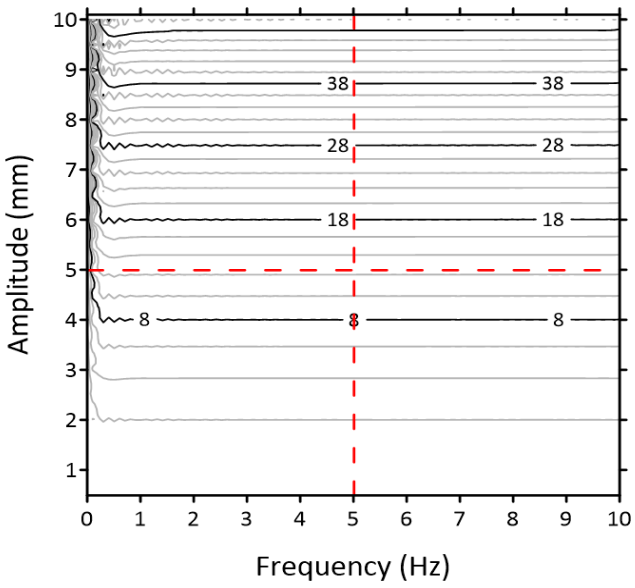

Figure 4.8a: Location of Cross-Sections for the Energy Algorithm

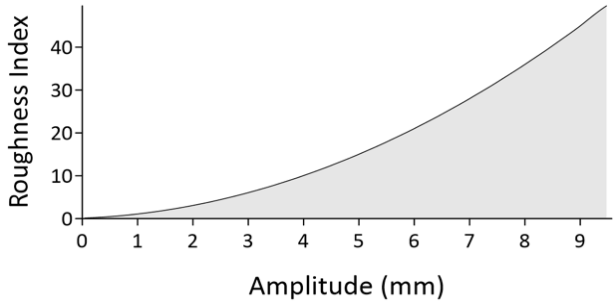

Figure 4.8b: Energy Roughness Indices at Constant 5 Hz Frequency

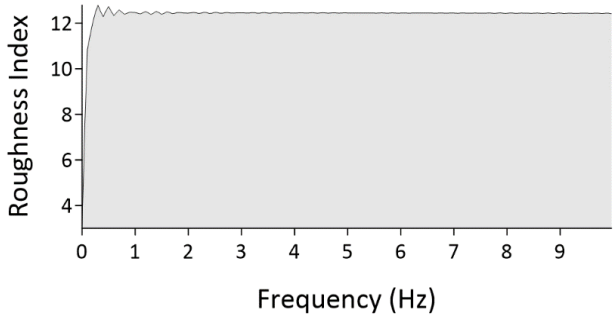

Figure 4.8c: Energy Roughness Indices at Constant 5 mm Amplitude
Figure 4.8 Cross-Sections from Energy Algorithm Plot

At a constant frequency, as shown in Figure 4.8b, the roughness indices increase non-linearly with increasing amplitude. The increase in roughness indices follows a second-degree

polynomial fit with a correlation coefficient of 1. This trend is true for frequencies between 1 Hz and 10 Hz.

At a constant amplitude, as shown in Figure 4.8c, the roughness indices increase rapidly from a frequency of 0.1 Hz to approximately 0.3 Hz. After the initial rise, there is a series of perturbations and an eventual leveling off of the roughness indices to a constant value. This trend can also be seen for profiles at other constant amplitudes.

4.2.3 Observations from Sinuosity Roughness Indices

The contour plot of the roughness indices as a function of amplitude and frequency for the Sinuosity algorithm is shown in Figure 4.9. This roughness algorithm outputs roughness indices that are on the order of 1. The maximum roughness index of 1.5483 occurred at the extreme case of an amplitude of 10 mm and a frequency of 10 Hz. The minimum roughness index, disregarding the baseline case, was found to be approximately 1 at an amplitude of 0.5 mm and a frequency of 0.1 Hz.

The shape of the contour lines follow a power curve trend with the inflection point aligned with a 45-degree line intersecting the origin to straight lines at high amplitude and frequency combinations. The contour lines appear straight because of the bounds of the contour plot. However, the contour lines are not symmetrical about the 45-degree line. For instance, at an amplitude of 9 mm and frequency of 3 Hz the roughness index is 1.0529 whereas at an amplitude of 3 mm and a frequency of 9 Hz the roughness index is 1.0531. The spacing of the contour lines decreases with increasing the combinations of amplitude and frequency indicating a non-linear increase in roughness indices.

A significant portion of the contour plot does not have any contour lines. This indicates a region where roughness indices are constant or change very slowly with increases in amplitude and frequency.

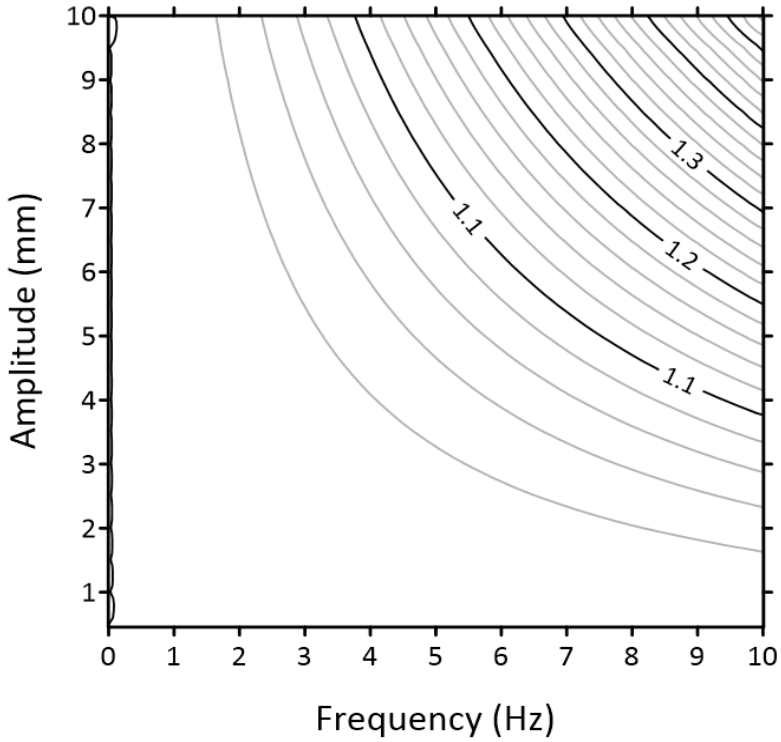

Figure 4.9 Sinuosity Roughness Indices as a Function of Amplitude and Frequency

The 3D surface plot was created to help better visualize the data and is shown Figure 4.10. It is easy to see the relatively constant region of roughness indices and the non-linear increase in roughness indices at extreme values of amplitude with relatively low frequencies, at extreme values of frequency with relatively low amplitude, and extreme values of both amplitude and frequency.

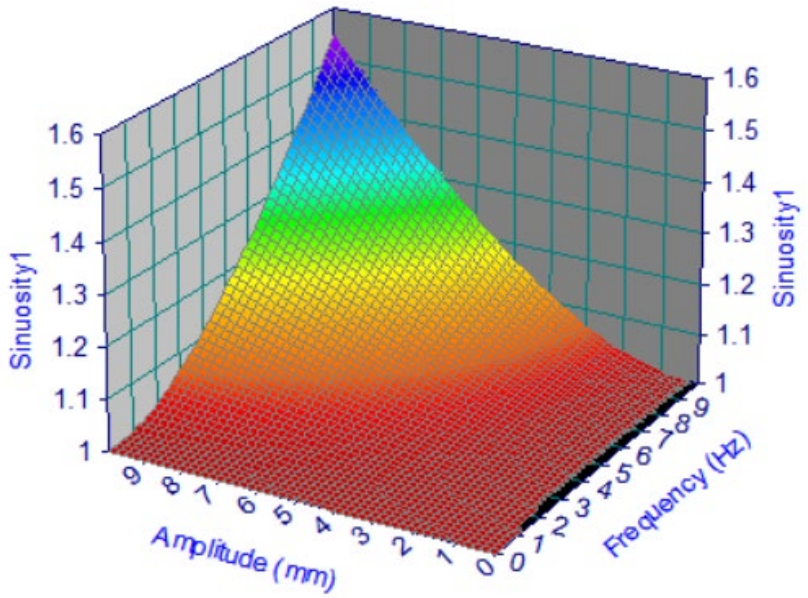

Figure 4.10 3D Visualization of Roughness Indices from Sinuosity Algorithm

To further investigate the effects of amplitude and frequency, a cross-section was taken along a 45-degree line running from the origin to an amplitude of 10 mm and a frequency of 10 Hz. This gives us paired combinations of amplitude and frequency with their respective roughness index. The cross-section location and resulting profile are shown in Figure 4.11. The cross-section in Figure 4.11b verifies the initial observation that the roughness index increases slowly as the combination of amplitude and frequency increases. At a paired amplitude of 3 mm and a frequency of 3 Hz, the increase in roughness indices follow a third-degree polynomial with a correlation coefficient of 0.99. This increase continues until it reaches the maximum roughness index of 1.5483 at an amplitude of 10 mm and a frequency of 10 Hz.

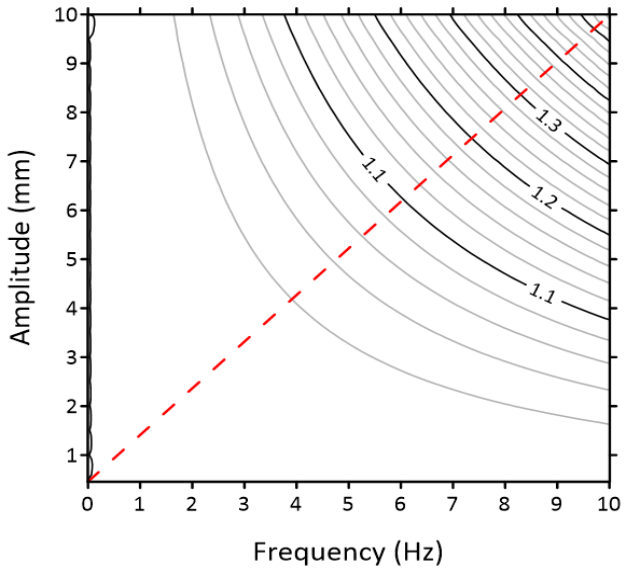

Figure 4.11a: Location of Cross-Section on Sinuosity Plot

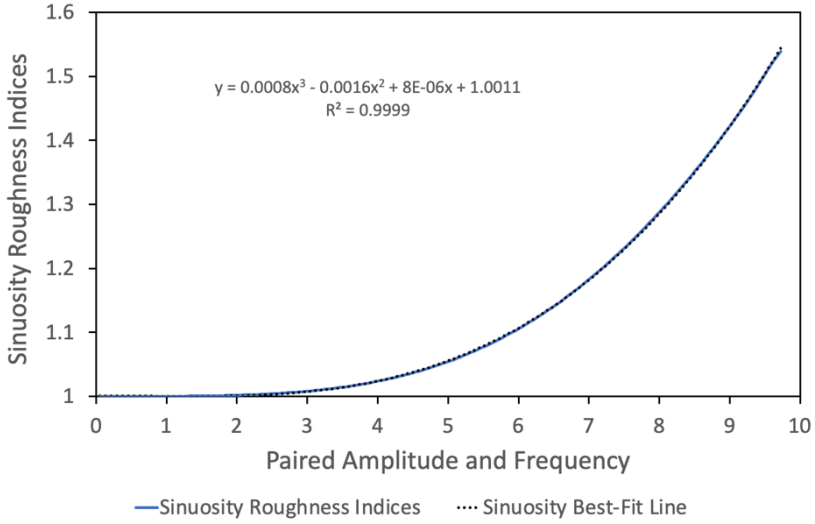

Figure 4.11b: Cross-Section of Sinuosity Roughness Indices at Paired Amplitudes and Frequencies of Sinuosity

Figure 4.11 Cross-Sections from Sinuosity Algorithm Plot

4.2.4 Observations from Z2 Roughness Indices

The contour plot of the roughness indices as a function of amplitude and frequency for the Z2 algorithm is shown in Figure 4.12. The magnitude of the roughness indices is relatively small with all values being on the order of one. The maximum roughness index of 1.2340 occurred at the extreme case of an amplitude of 10 mm and a frequency of 10 Hz. The minimum

roughness index, disregarding the baseline case, was found to be 0.0005857 at an amplitude of 0.5 mm and a frequency of 0.1 Hz. The shape of the contours is similar to those of the Sinuosity algorithm (Figure 4.9).

The shape of the contour lines follow a power curve trend with the inflection point approximately aligned with a 45-degree line intersecting the origin to straight lines at high amplitude and frequency combinations. The straight lines on the plot appear to be straight because of the bounds that were set on the contour plot. The spacing of the contour lines decreases with increasing the combinations of amplitude and frequency indicating a non-linear increase in roughness indices.

A small portion of the contour plot, notably in the lower left-hand side, does not have any contour lines. This indicates a region where roughness indices are constant or change very slowly with increases in amplitude and frequency.

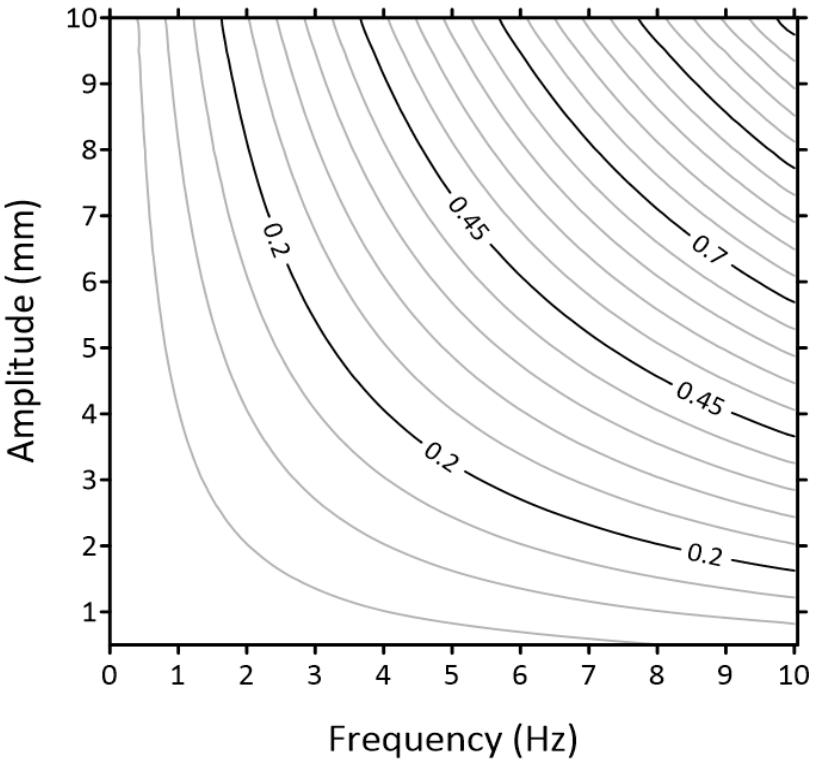

Figure 4.12 Z2 Roughness Indices as a Function of Amplitude and Frequency

A 3D surface plot corresponding to the data presented in Figure 4.12 is shown in Figure 4.13. In the 3D plot, it is easy to see the relatively small region of constant values of roughness indices and the non-linear increase in roughness indices.

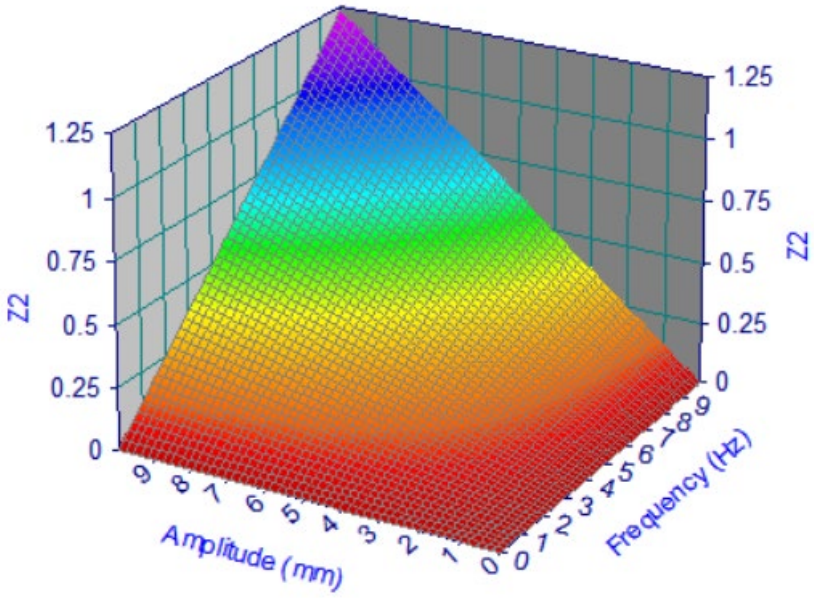

Figure 4.13 3D Visualization of Roughness Indices from Z2 Algorithm

The effects of amplitude and frequency on roughness are evident in a cross-section along a 45-degree line running from the origin to an amplitude of 10 mm and a frequency of 10 Hz. This cross-section line gives us paired combinations of amplitude and frequency with their respective roughness indices. The cross-section location and resulting profile are shown in Figure 4.14. The cross-section, Figure 4.14b, verifies that as the combination of amplitude and frequency increases the increase of the roughness index is exponential. There is a small region, approximately 0.1 to 1 of paired amplitude and frequency, where the roughness indices are constant. After this region, the increase in roughness indices follows a third-degree polynomial with a correlation coefficient of 1. This increase occurs until the maximum roughness index of 1.234 at an amplitude of 10 mm and a frequency of 10 Hz.

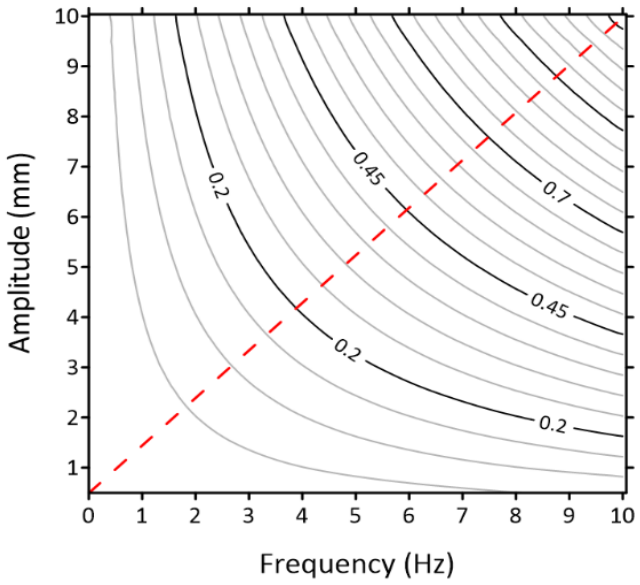

Figure 4.14a: Location of Cross-Section on Z2 Plot

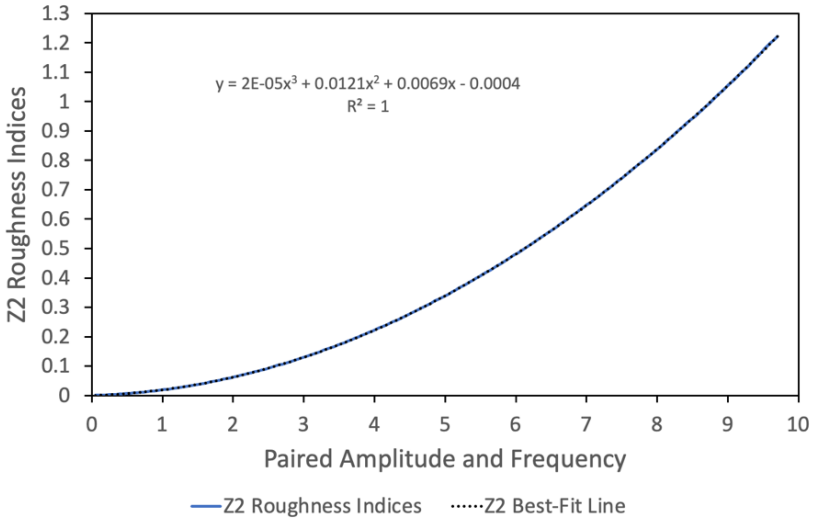

Figure 4.14b: Cross-Section of Sinuosity Roughness Indices at Paired Amplitudes and Frequencies

Figure 4.14 Location and Cross-Section from Z2 Algorithm Plot

4.2.5 Observations from Mean Absolute Angle (MAA) Roughness Indices

The contour plot of the roughness indices as a function of amplitude and frequency from the mean absolute angle (MAA) algorithm is shown in Figure 4.15. The roughness algorithm

outputs very small values of roughness indices with all the values being less than one. The maximum roughness index of 0.7969 occurred at the extreme case of an amplitude of 10 mm and a frequency of 10 Hz. The minimum roughness index, disregarding the baseline case, was found to be 0.000273 at an amplitude of 0.5 mm and a frequency of 0.1 Hz. The shape of the contours is similar to those of the Sinuosity (Figure 4.9) and Z2 (Figure 4.12) algorithms.

The shape of the contour lines follow a power curve trend with the inflection point approximately aligned with a 45-degree line intersecting the origin to straight lines at high amplitude and frequency combinations. The spacing of the contours stays relatively constant after the 0.2 contour line.

For this algorithm, the area with little to no change of roughness index as a function of amplitude and frequency extends from the origin upward along the y-axis. This indicates a region where roughness indices are constant or change very slowly with increases in amplitude and frequency.

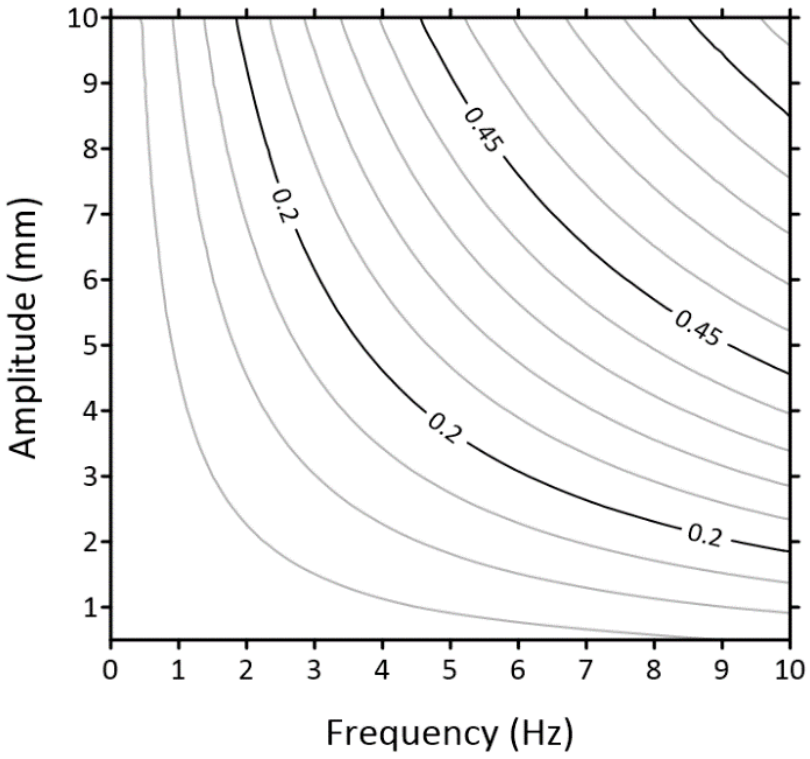

Figure 4.15 Mean Absolute Angle Roughness Indices as a Function of Amplitude and Frequency

In the 3D surface plot shown in Figure 4.16, it is easy to see the relatively small region of constant values of roughness indices and the non-linear increase in roughness indices.

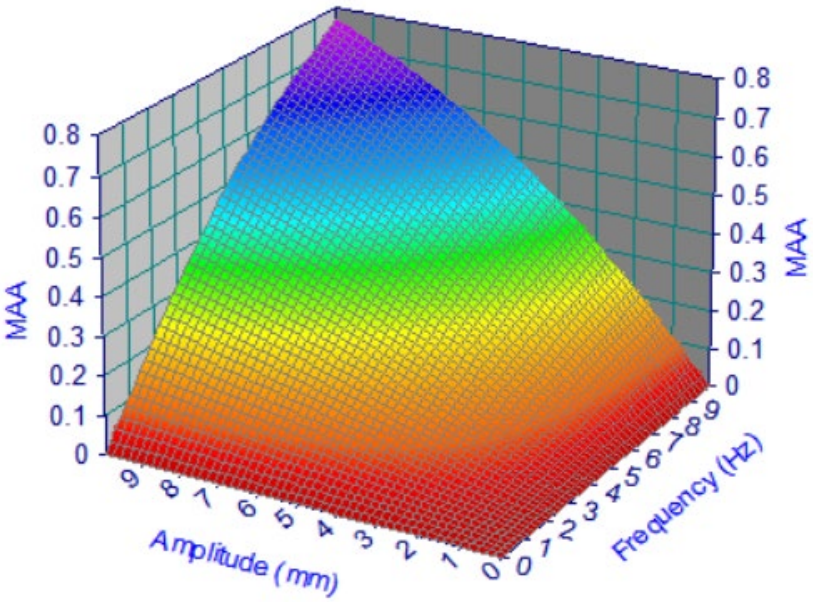

Figure 4.16 3D Visualization of Roughness Indices from MAA Algorithm

In the cross-section taken along a 45-degree line running from the origin to an amplitude of 10 mm and a frequency of 10 Hz, shown in Figure 4.17, roughness indices increase non-linearly and then increase linearly with an increase in paired amplitude and frequency. The transition between non-linear and linear increase occurs at approximately 1 Hz. The increase of roughness indices follows a third-degree polynomial with a correlation coefficient of 1. This increase occurs until the maximum roughness index of 0.7969 is achieved at an amplitude of 10 mm and a frequency of 10 Hz.

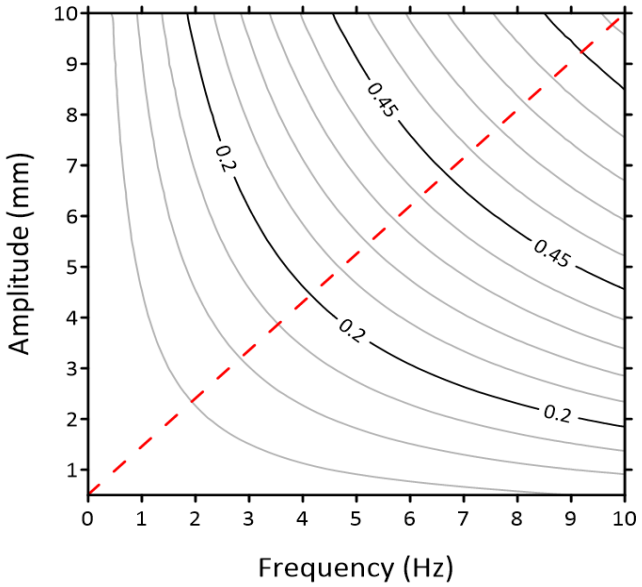

Figure 4.17a: Location of Cross-Section on MAA Plot

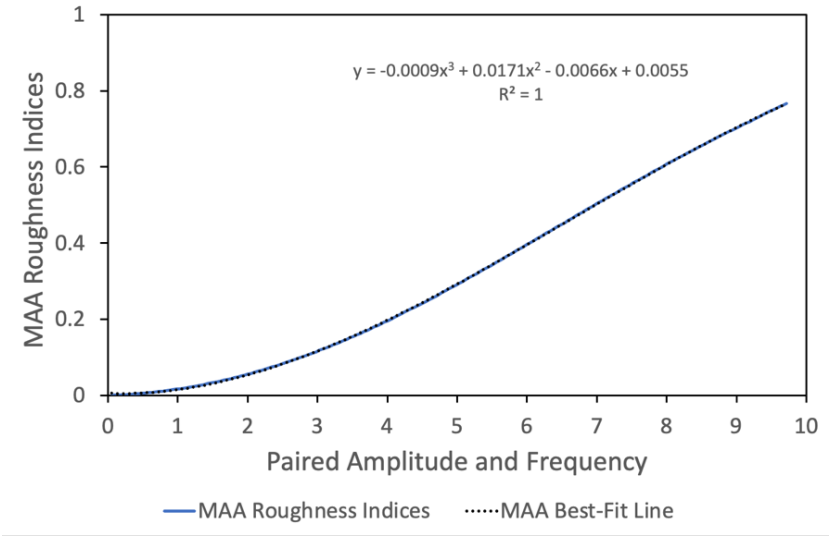

Figure 4.17b Cross-Section of MAA Roughness Indices at Paired Amplitudes and Frequencies

Figure 4.17 Location and Cross-Section from MAA Algorithm Plot

4.2.6 Observations from Modified Divider a-Value

The contour plot of the Modified Divider a-Value as a function of amplitude and frequency is shown in Figure 4.18. The maximum roughness index of 3.1881 occurred at the extreme case of an amplitude of 10 mm and a frequency of 10 Hz. The minimum roughness index, disregarding the baseline case, was found to be 2.996 at an amplitude of 0.5 mm and a frequency of 0.1 Hz. The shape of the contours is similar to those of the Sinuosity (Figure 4.9), Z2 (Figure 4.12), and MAA (Figure 4.15) algorithms.

The shape of the contour lines follow a power curve trend with the inflection point approximately aligned with a 45-degree line intersecting the origin to straight lines at high amplitude and frequency combinations. The spacing of the contour lines decreases with increasing the combinations of amplitude and frequency up to approximately the 3.05 contour level. After this contour level, the contour lines are approximately equally spaced.

A portion of the contour plot, notably in the lower left-hand side, does not have any contour lines. This indicates a region where roughness indices are constant or change very slowly with increases in amplitude and frequency.

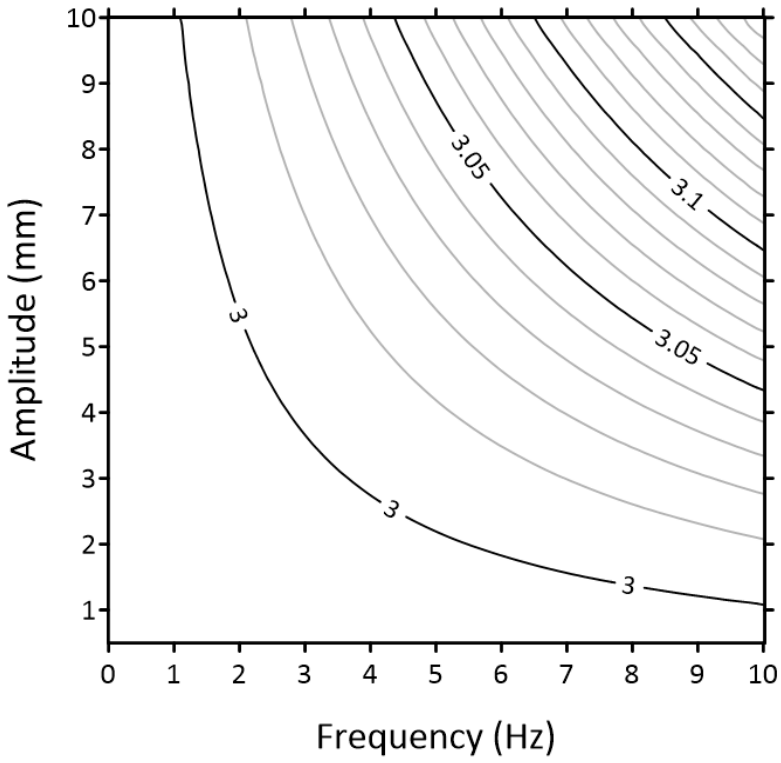

Figure 4.18 Modified Divider a-Value as a Function of Amplitude and Frequency

A 3D surface plot was created and shown in Figure 4.19. This plot has the same x- and y-axes as the contour plot but the roughness indices are plotted as a surface. It is easy to see the relatively large region of constant a-values and then an increase of a-values with increasing amplitude and frequency.

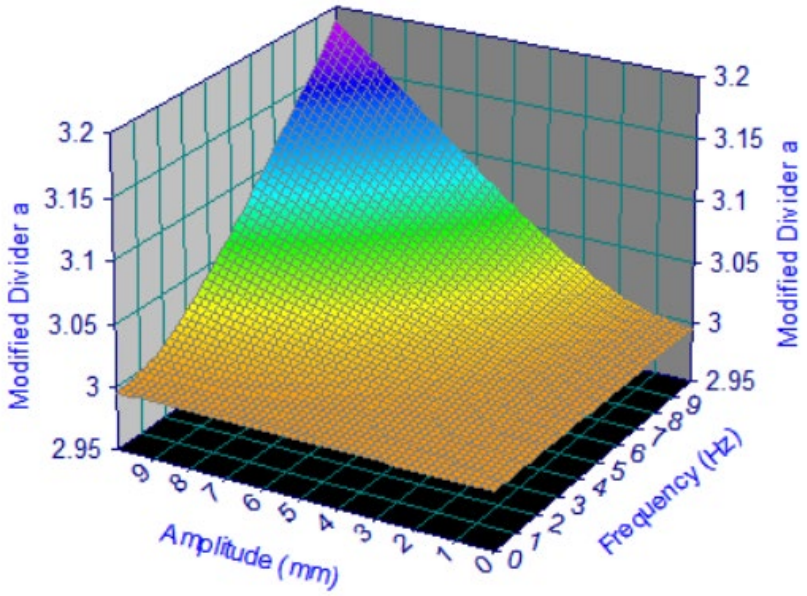

Figure 4.19 3D Visualization of a Value from Modified Divider Algorithm

In the cross-section taken along a 45-degree line running from the origin to an amplitude of 10 mm and a frequency of 10 Hz, shown in Figure 4.20, it may be seen that the a-values are constant in the range between 0.1 and 4 paired values of amplitude (mm) and frequency (Hz). There is a non-linearly increasing portion of a values to approximately 8.5, after which the a-Values increase linearly. The increase of roughness indices follows a third-degree polynomial with a correlation coefficient of 0.99. The increase continues until the maximum roughness index of 3.18 is achieved at an amplitude of 10 mm and a frequency of 10 Hz.

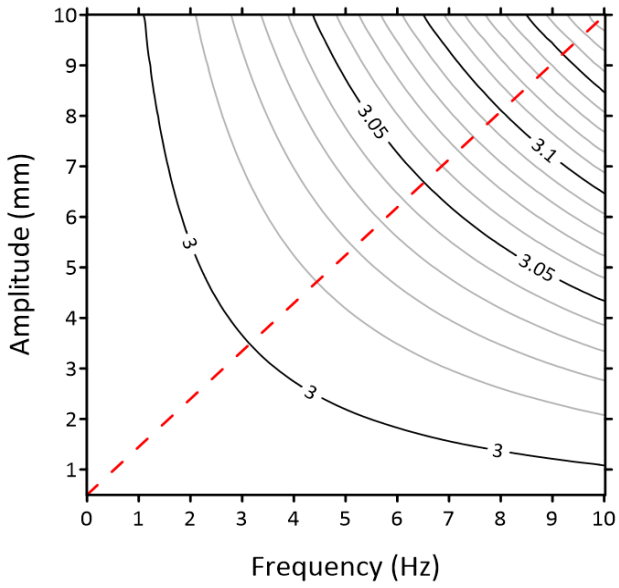

Figure 4.20a: Location of Cross-Section on Modified Divider a-Value Plot

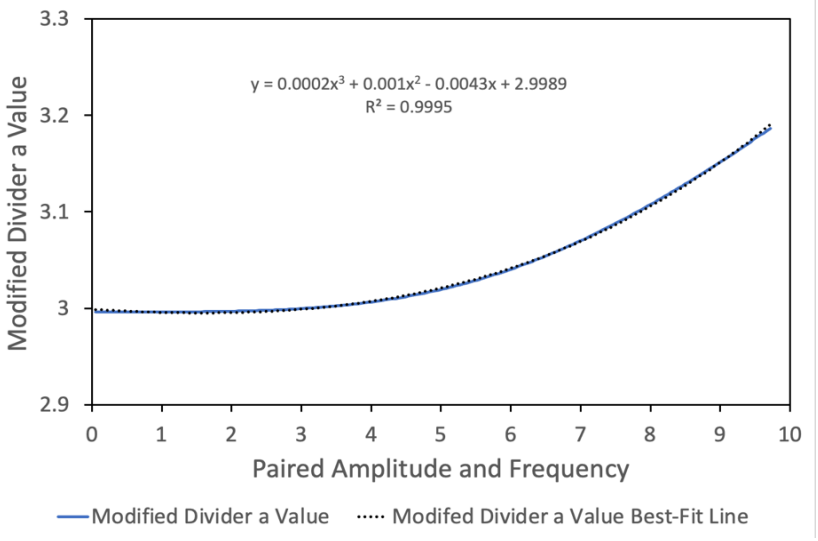

Figure 4.20b: Cross-Section of Modified Divider a-Value at Paired Amplitudes and Frequencies

Figure 4.20 Location and Cross-Section from Modified Divider a-Value Plot

4.2.7 Summary of Observations

Based on observations from the contour plots of roughness indices and fractal intercept as a function of amplitude and frequency, we can find the influences of amplitude, frequency, or a combination of both on the output index and intercept. The visualization of these algorithms shows the attitude of how these indices increase and by what terms they increase. These

visualizations will be used to help determine relationships between the different algorithms and will later lead to finding equations linking algorithms. Table 4.1 highlights observations that were made of the roughness indices for each of the roughness algorithms. This table features the maximum and minimum roughness indices as well as the locations where these values are found.

Table 4.1 Maximum and Minimum Roughness Indices from Roughness Algorithms

Algorithm	Roughness Index			
	Maximum and Location		Minimum and Location	
RMS	7.2988	10 mm 0.3 Hz	0.15	0.5 mm 0.1 Hz
Energy	54.708	10 mm 0.1 Hz	0.1139	0.5 mm 0.2 Hz
Sinuosity	1.5483	10 mm 10 Hz	1.00000005	0.5 mm 0.1 Hz
Z2	1.2340	10 mm 10 Hz	0.0005857	0.5 mm 0.1 Hz
Mean Absolute Angle	0.7696	10 mm 10 Hz	0.000273	0.5 mm 0.1 Hz
Modified Divider a-Value	3.1881	10 mm 10 Hz	2.996	0.5 mm 0.1 Hz

Numerous observations and trends are contained within Table 4.1. First, the range of roughness indices varies for all roughness algorithms. The Energy algorithm has the greatest range of roughness indices with values ranging between 0.114 to 54.7. It is noteworthy that Energy has the highest roughness index with its value being seven times that of that the next largest roughness index. The algorithm with the smallest range of roughness indices is the Modified Divider a-Value with its range being 2.99 to 3.19.

Table 4.1 also highlights the location where the maximum and minimum roughness indices occur. The maximum roughness index occurs at the extreme case, amplitude of 10 mm

and a frequency of 10 Hz, for all roughness algorithms except RMS and Energy. The maximum roughness for RMS and Energy algorithms occurs at low amplitudes and low frequencies. These two algorithms also have similar minimum roughness indices.

The maximum roughness indices of Sinuosity and Z2 algorithms are similar, 1.5483 and 1.2340, respectively. The minimum roughness indices for RMS, Energy, Sinuosity, and Modified Divider a-Value algorithms are on the same order of magnitude, whereas the minimum roughness index for MAA and Z2 is one order of magnitude lower. They are both approximately zero. It is to be noted that all values within this table are a function of the step sizes used for each of the parameters.

4.3 Chapter Summary

Contour plots of roughness indices and fractal intercept values were visualized as a function of amplitude and frequency. These plots are useful to understand the attitude of the roughness indices at different combinations of amplitude and frequency and where roughness indices increase linearly or non-linearly.

To further examine how roughness indices vary with amplitude and frequency, cross-sections were taken at either the midpoints of the amplitude and frequency range (RMS and Energy algorithms) or along a 45-degree line running from the origin to an amplitude of 10 mm and a frequency of 10 Hz (Sinuosity, Z2, MAA, Modified Divider a-Value). RMS and Energy cross-sections showed the same general trends. At a constant amplitude, the roughness indices increased rapidly and became constant after approximately 1 Hz. At a constant frequency, above 1 Hz, RMS had a linear increase of roughness indices for increasing amplitudes, but Energy had a non-linear increase in roughness indices with increasing amplitudes. Sinuosity, Z2, MAA, and Modified Divider a-Values roughness indices increased non-linearly with paired increases of amplitude and frequency.

The Energy roughness algorithm has the largest range of roughness indices and the highest maximum roughness index with values ranging from 0.11-54.7. The Modified Divider a-Value algorithm has the smallest range of values ranging from 2.99-3.18. The locations of the maximum roughness index occur at the extreme case of an amplitude of 10 mm and a frequency of 10 Hz for all the algorithms except RMS and Energy, where the maximum roughness index occurs at low frequency combinations. Maximum roughness index values were very similar for the Sinuosity and Z2 algorithms and the minimum roughness index values were very similar for the RMS and Energy algorithms.

CHAPTER FIVE: COMPARATIVE RELATIONSHIP BETWEEN ROUGHNESS ALGORITHMS

This chapter answers the research question “Is it possible to establish a comparative relationship between roughness indices and fractal intercepts from different algorithms?”. Roughness indices and fractal intercepts have been plotted on contour plots to visualize relationships between amplitude and frequency. Observations and data trends have been made using the contour plots and cross-sections made at select locations. This chapter presents how and why roughness algorithms have been paired together and comparisons between visualizations are presented.

5.1 Grouping of Algorithms

The initial observations from the roughness indices or fractal intercept from each of the algorithms were presented in Chapter 4. When looking at contour plots, it was readily apparent which contour plots exhibited similar trends. The first grouping of algorithms is Root Mean Square (RMS) and Energy. The second grouping of algorithms is Sinuosity, Z2, Mean Absolute Angle, and Modified Divider a-Value.

5.2 RMS and Energy Roughness Algorithm Pair

Figure 5.1 presents the roughness indices of RMS (Figure 5.1a) and Energy (Figure 5.1b) as a function of amplitude and frequency. These two algorithms were paired because of the similarities in the shape of the contour plots. At constant amplitudes, there is a rapid increase in roughness indices at low frequencies (between 0.1 Hz to approximately 0.3 Hz) followed by a series of perturbations of roughness indices until the roughness index reaches a constant value.

For the same frequency, higher amplitudes have a steeper rise in roughness algorithms and higher and longer series of perturbations.

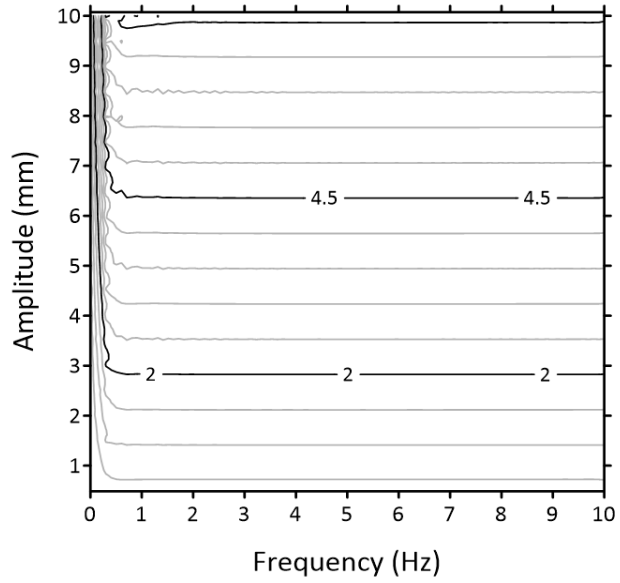

Figure 5.1a: RMS Roughness Indices as a Function of Amplitude and Frequency

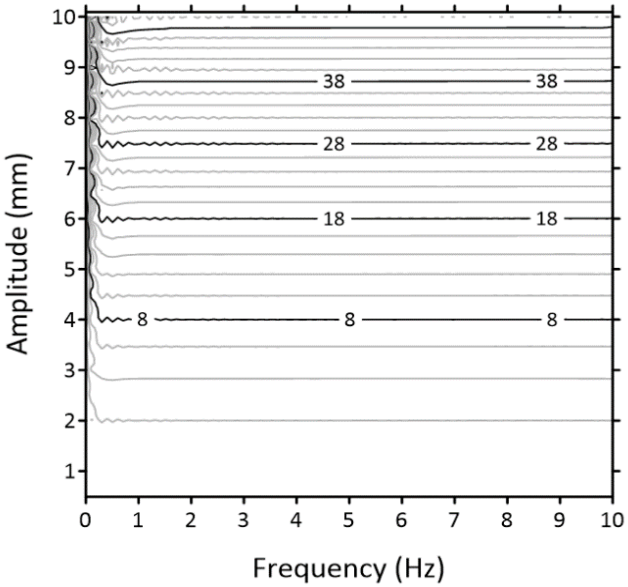

Figure 5.1b: Energy Roughness Indices as a Function of Amplitude and Frequency

Figure 5.1 Comparison of Roughness Indices as a Function of Amplitude and Frequency Between RMS and Energy Algorithms

Although the similarities are remarkable, there are some differences. The main difference between the two algorithms is the magnitude of the roughness index. Roughness indices for the Energy algorithm ranged between 0.1139 and 54.708 whereas the roughness indices from the RMS algorithm ranged between 0.15 and 7.2988. These minimum and maximum values occurred at approximately the same amplitudes and frequencies.

The difference in magnitudes is attributed to the effect of amplitude. At constant frequencies, the RMS roughness indices vary linearly with amplitude. On the contour plot, this is indicated by equally spaced contour lines. However, at constant frequencies, the Energy roughness indices vary non-linearly with increasing amplitude. The roughness indices computed using the Energy algorithm are more sensitive to amplitude than RMS roughness indices.

5.3 Sinuosity, Z2, MAA, and Modified Divider a-Value Algorithm Group

Figure 5.2 presents the roughness indices and fractal intercept values as a function of amplitude and frequency. At first glance, it is readily apparent why these algorithms were grouped together. The roughness indices and the fractal intercept follow the same general trend. The contours are generally follow a power curve trend with the inflection point roughly aligned with the maximum roughness value that is located at an amplitude of 10 mm and a frequency of 10 Hz. As noted in Table 4.1, the minimum roughness index or fractal intercept occurred at an amplitude of 0.5 mm and a frequency of 0.1 Hz. Additionally, all plots show some level of white space, or absence of contour lines, at the lower left-hand corner of the contour plot. The white space indicates roughness indices or fractal intercept values are constant or only slightly changing with amplitude and frequency.

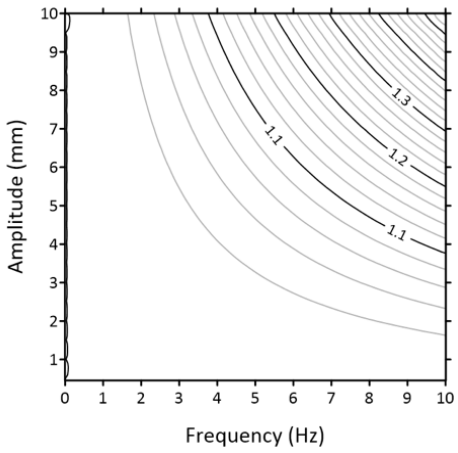

Figure 5.2a: Sinuosity

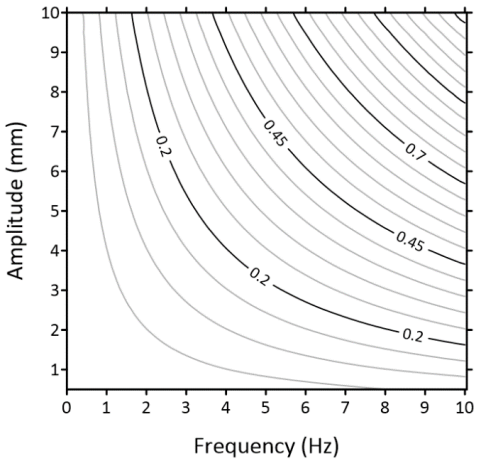

Figure 5.2b: Z2

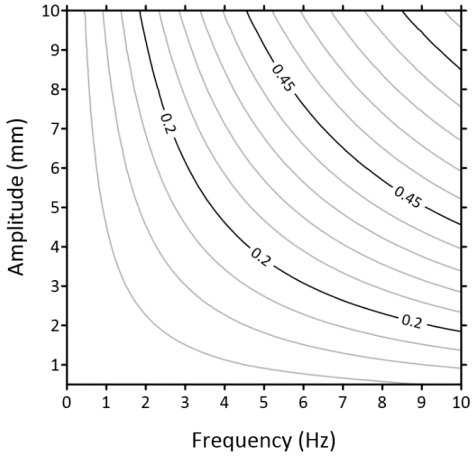

Figure 5.2c: MAA

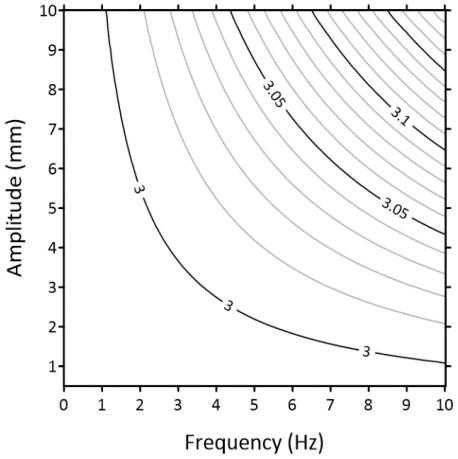

Figure 5.2d: Modified Divider a-Value

Figure 5.2 Comparison of Roughness Indices and Fractal Intercept as a Function of Amplitude and Frequency Between Sinuosity, Z2, MAA, and Modified Divider Algorithms

There are differences between the contour plots that lead to a subgrouping or pairing of these algorithms. The first difference is the shape of the first contour. The first contour line of the MAA and Z2 plots is a sweeping L shape that intersects the x-axis at a value less than 10 Hz. The first contour line of the Sinuosity and Modified Divider a-Value is a semi-circular shape that does not intersect the x-axis or y-axis. The second difference between these four plots is the area of white space beneath the first contour line. Figure 5.3 shows the first contour line for each of the

contour plots. The first contour line was the result from ordinary kriging used to develop the contour plots.

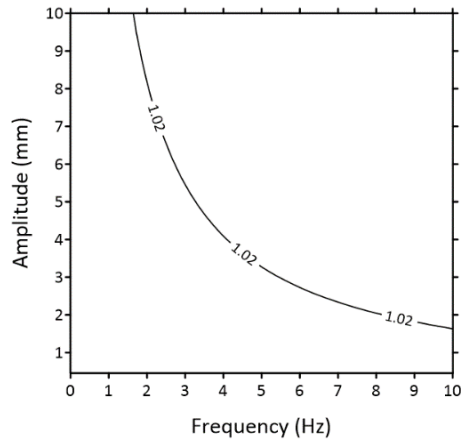

Figure 5.3a: Sinuosity

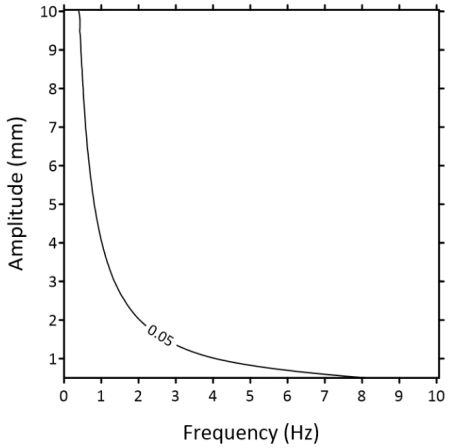

Figure 5.3b: Z2

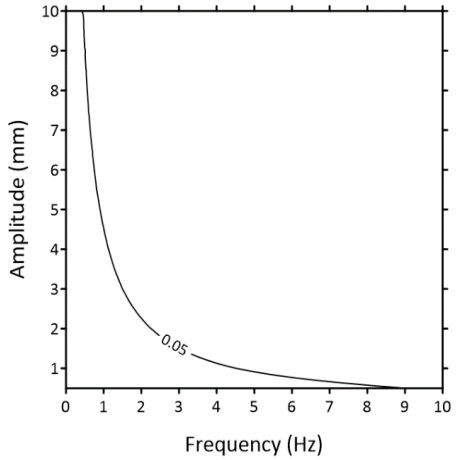

Figure 5.3c: MAA

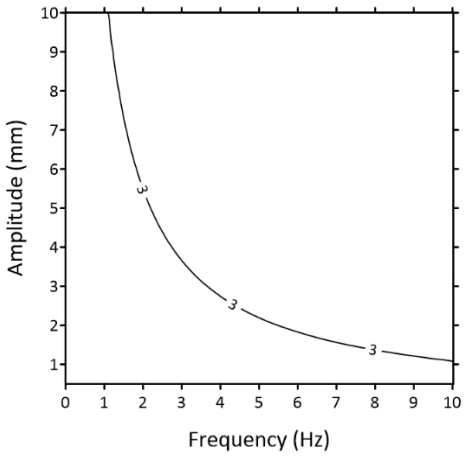

Figure 5.3d: Modified Divider a-Value

Figure 5.3 First Contour Line of the Roughness Index and a-Value as a Function of Amplitude and Frequency

The approximate planar area percentage beneath the first contour line for Z2 and MAA, and for Sinuosity and Modified Divider a-Value is similar. The approximate planar area percentage is 13.59 for MAA and 12.22 for Z2. The approximate planar area percentage is 40.98 for Sinuosity and 30.19 for the Modified Divider a-Value.

The common shapes of the initial contours and the commonalities in the white space planar area prompted a pairing of roughness algorithms. Moving forward, the Z2 and MAA algorithms are paired, and the Sinuosity and Modified Divider a-Value algorithms are paired.

5.4 Chapter Summary

Observations were made from contour plots of roughness indices as a function of amplitude and frequency. Based on the shape of the contours, the spacing of the contours, and the magnitude of the roughness indices, the roughness algorithms were divided into two groups. The first group, or pairing, was RMS and Energy algorithms. The roughness indices contour plots for these algorithms both showed a rapid increase in roughness indices at low frequencies and plateau of constant roughness indices. At a constant frequency, the increase in roughness indices with increasing amplitude is linear.

The second group consisted of Sinuosity, Z2, MAA, and Modified Divider a-Value algorithms. The roughness indices contours showed sweeping power curve trends with inflection points that were roughly aligned along a 45-degree line with the origin of the plot. However, the magnitude of the roughness indices and the specific shape of the first contour created a natural subdivision within this group. Due to their similarities, the Sinuosity and Modified Divider a-Value algorithms were paired and Z2 and MAA algorithms were paired.

CHAPTER SIX: EQUATIONS LINKING ROUGHNESS INDICES

This chapter answers the research question "Is it possible to develop an equation to relate the most often used roughness algorithms?". The six algorithms have been placed into three pairings: RMS and Energy, Z2 and MAA, and Sinuosity and Modified Divider a-Value. This chapter presents the methodology of developing equations between paired algorithms. The first step in the process was to fit a surface to the roughness indices and compute the percentage difference between the roughness indices and the equation determined roughness indices. To develop an equation linking paired algorithms, a translation factor was determined using the roughness indices of the paired algorithms. An equation was fit to the translation factor. This equation could then be used to predict one algorithm as a function of amplitude, frequency, and the roughness index. Finally, equation derived roughness indices were compared to the roughness indices.

6.1 Determination of the Best-Fit Surface of Roughness Algorithms

To develop equations to link paired algorithms, roughness indices must be represented by a best-fit surface. For each algorithm, a surface was fit to the roughness indices and the equation of the surface was compared to the roughness index at each amplitude and frequency.

To determine the best-fit surface to the roughness indices, TableCurve 3D by Systat Software Inc. was used. Within TableCurve 3D, polynomial equations were chosen to fit the roughness indices. To choose the best-fit equation to represent the data, the simplest equation with the highest correlation coefficient was chosen. A perfect positive correlation coefficient is 1.0 with the lowest correlation coefficient for the six roughness algorithms being 0.9825. To

assess the best-fit surface, a percentage difference calculation was performed. The equation used was:

$$Percentage\ Difference = \frac{|Fit\ Data - Algorithm\ Data|}{\left(\frac{Fit\ Data + Algorithm\ Data}{2}\right)} \times 100 \qquad \textbf{Equation 6.1}$$

A percentage difference of five percent was chosen as the tolerable difference. Contour plots showing the tolerable difference were produced.

6.1.1 Best-Fit Surfaces for RMS and Energy Roughness Indices

Figure 6.1 shows the contour plot for the RMS roughness indices (Figure 6.1a), the best-fit surface for the roughness indices (Figure 6.1b), and the percentage difference contour plot between the roughness indices and the best-fit surface (Figure 6.1c). The equation for the best-fit surface is:

$$z_{RMS} = 0.1377 + 0.1816\ln(x) + 0.6608y + 0.1439(\ln(x))^2 - 4.5084 \times 10^{-9}y^2 + 0.0296y\ln(x) - 0.0002(\ln(x))^3 + 2.4503 \times 10^{-10}y^3 - 1.3664 \times 10^{-12}y^2\ln(x) + 4.1362 \times 10^{-5}y(\ln(x))^2 \qquad \textbf{Equation 6.2}$$

The correlation coefficient for the equation is 0.9911.

Although the correlation coefficient is very high, there are noticeable differences between the contour plots in Figure 6.1a and Figure 6.1b. At low frequencies, the roughness indices have a very steep rise to horizontally oriented contour lines. The best-fit surface fails to capture the steep rise at low frequencies. The contour lines for the best-fit surface are not horizontal but are inclined towards the origin of the contour plot. This is especially noticeable at low frequencies.

In general, the best-fit surface accurately represents the roughness indices at frequencies greater than 1 Hz and amplitudes greater than 3 mm, as shown in the percentage difference contour plot (Figure 6.1c). The percentage difference of 5% is shown and percentage differences above 5% are highlighted. There are two hump shaped features at the bottom of the plot where

the percentage difference is greater than five percent. These areas correspond to the areas where the contour lines of the best-fit surface inclined towards the origin. The approximate planar area below the 5% contour is 71.86% indicating the best surface adequately represents approximately 72% of the roughness indices.

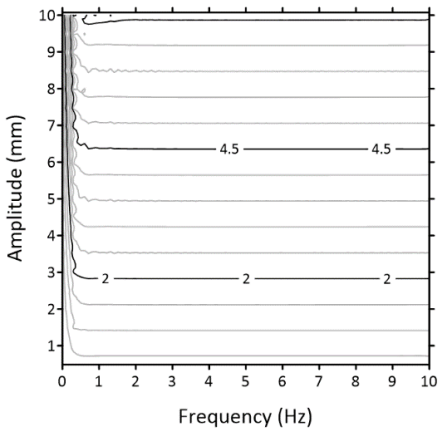

Figure 6.1a: RMS Roughness Indices Contour Plot

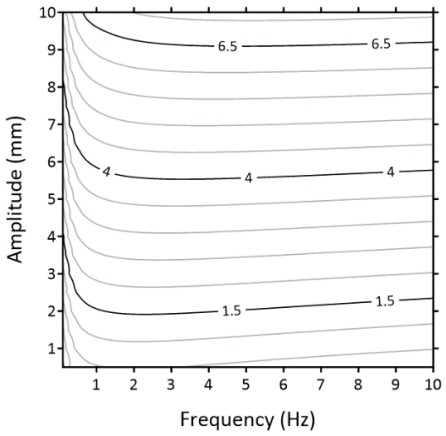

Figure 6.1b: Best-fit Surface for RMS Roughness Indices

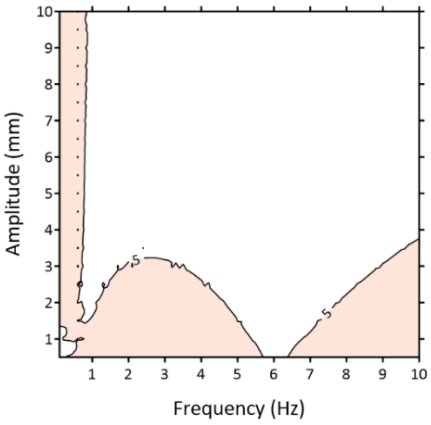

Figure 6.1c: Percentage Difference RMS Contour Plot with 5% Tolerance Contour

Figure 6.1 Contour Plots of RMS Roughness Indices, Fitted Surface to the Roughness Indices, and the Percentage Difference Between Roughness Indices and the Fitted Surface

Figure 6.2 shows the contour plot for the Energy roughness indices (Figure 6.2a), the best-fit surface for the roughness indices (Figure 6.2b), and the percentage difference between the roughness indices and the best-fit surface (Figures 6.2c). The equation for the best-fit surface is:

$$z_{Energy} = -0.1036 - 0.02597\ln(x) + 0.02924y + 0.05234(\ln(x))^2 - 0.499y^2 - 0.02182y\ln(x) + 7.583 \times 10^{-5}(\ln(x))^3 + 1.165 \times 10^{-9}y^3 - 0.00072y^2\ln(x) - 3.1659 \times 10^{-5}y(\ln(x))^2 \quad \textbf{Equation 6.3}$$

The correlation coefficient for the equation is 0.9991.

Although the correlation coefficient is very high, there are slight differences between the contour plot of the roughness indices and the best-fit surface. The perturbations at low frequencies in the roughness indices plot are smoothed in the best-fit surface plot. Also, the steep rise at very low frequencies is more pronounced in the best-fit surface plot than the roughness indices plot.

In general, the best-fit surface accurately represents the roughness indices at frequencies greater than 0.5 Hz and amplitudes greater than 1.75 mm, as shown in the percentage difference contour plot (Figure 6.2c). These differences are very similar to those described for the RMS percentages differences plot. The percentage difference of 5% is shown and percentage differences above 5% are highlighted. There are two hump shaped features at the bottom of the plot where the percentage difference is greater than five percent. The approximate planar area below the 5% contour is 82.58% indicating the best-fit surface adequately represents approximately 83% of the roughness indices.

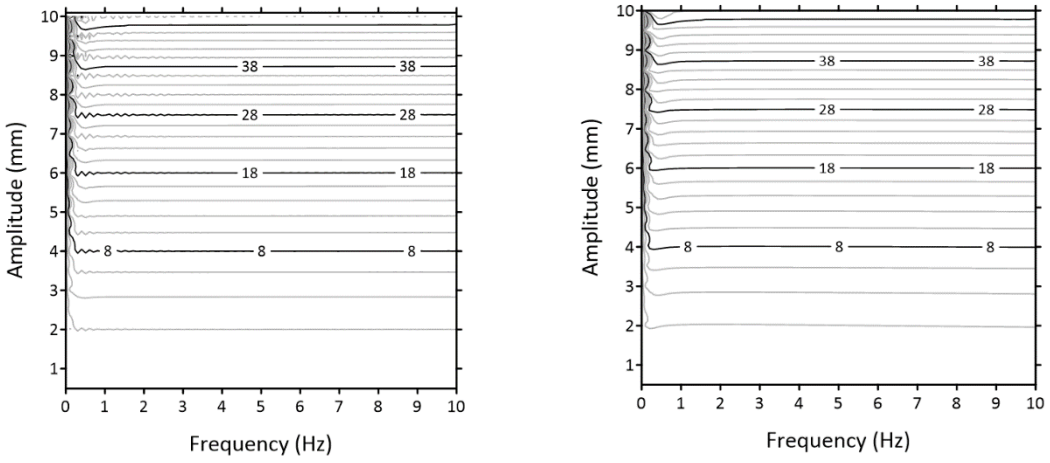

Figure 6.2a: Energy Roughness Indices Contour Plot **Figure 6.2b: Best-fit Surface for Energy Roughness Indices**

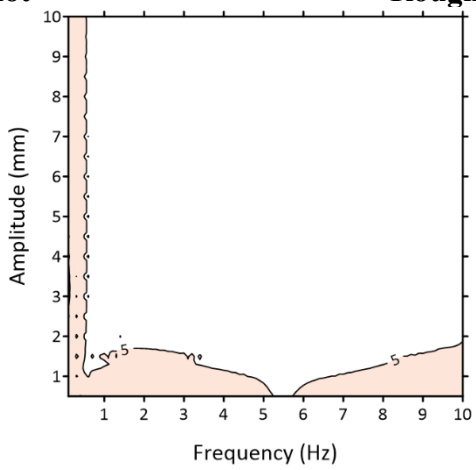

Figure 6.2c: Percentage Difference Energy Contour Plot with 5% Tolerance Contour

Figure 6.2 Contour Plots of Energy Roughness Indices, Fitted Surface to the Roughness Indices, and the Percent Difference Between Roughness Indices and the Fitted Surface.

When looking at the best-fit surfaces that were found for RMS and Energy, we can see that in both plots the roughness indices have the greatest percent difference at frequencies less than 1 Hz and amplitudes less than 2 mm. This tells us that in these regions it may be difficult to accurately relate these two algorithms due to the variation of values. The best-fit surface for Energy did a much better job at representing the data with approximately 82.58% of the data being accurately represented where 71.86% was accurately represented for RMS.

6.1.2 Best-Fit Surfaces for Sinuosity and Modified Divider a-Value Indices

Figure 6.3 shows the contour plots for the Sinuosity roughness indices (Figure 6.3a), the best-fit surface for the roughness indices (Figure 6.3b), and the percentage difference contour plot between the roughness indices and the best-fit surface (Figure 6.3c). The equation for the best-fit surface is:

$$z_{Sinuosity} = 1.0754 - 0.02817x - 0.02641y + 0.00182x^2 + 0.0017y^2 + 0.00617xy$$

Equation 6.4

The correlation coefficient for the equation is 0.9825.

Although the correlation coefficient is very high, there are still noticeable differences between the contour plots seen in Figure 6.3a and Figure 6.3b. At low frequency and amplitude values, the best-fit surface shows a gentle rise in estimated roughness indices which is not present in the actual roughness indices. The best-fit surface equation has trouble accurately depicting the values at low frequency and amplitude combinations. The best-fit surface has the lowest contour of 1.0 whereas the contour plot for actual roughness indices has a lowest contour of 1.02 because the lowest roughness index for the Sinuosity algorithm is slightly greater than one.

In general, the best-fit surface accurately represents the roughness indices at frequencies greater than 0.5 Hz and amplitudes greater than 1 mm, as shown in the percent difference contour plot (Figure 6.3c). The percentage difference contour of 5% is shown and the percentage difference above 5% is highlighted. There is a very small portion at extreme low values of amplitude and frequency that is highlighted. The approximate planar area below the 5% contour is 94.88% indicating that the best-fit surface adequately represents approximately 95% of the roughness indices.

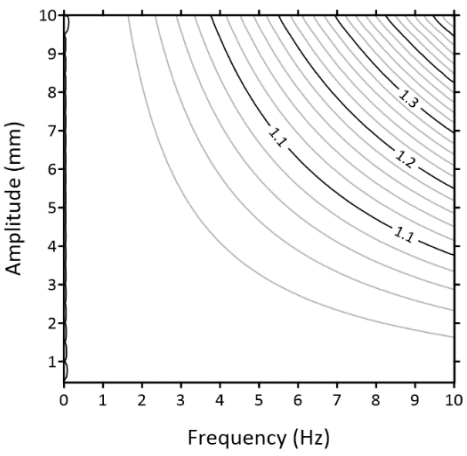

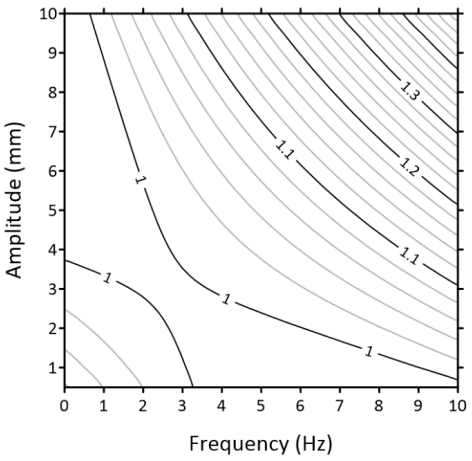

Figure 6.3a: Sinuosity Roughness Indices Contour Plot

Figure 6.3b: Best-fit Surface for Sinuosity Roughness Indices

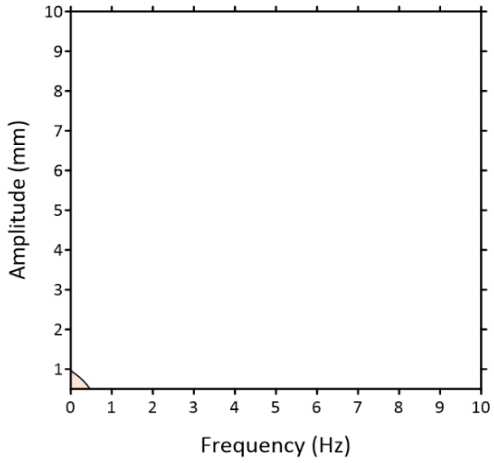

Figure 6.3c: Percentage Difference Sinuosity Contour Plot with 5% Tolerance Contour

Figure 6.3 Contour Plots of Sinuosity Roughness Indices, Fitted Surface to the Roughness Indices, and the Percent Difference Between Roughness Indices and the Fitted Surface.

Figure 6.4 shows the contour plots for the Modified Divider a-Value roughness indices (Figure 6.4a), the best-fit surface for the roughness indices (Figure 6.4b), and the percentage difference contour plot between the roughness indices and the best-fit surface (Figure 6.4c). The equation for the best-fit surface is:

$$z_{MDA} = 3.0192 - 0.009206x - 0.008358y + 0.000595x^2 + 0.0005195y^2 + 0.002264xy \quad \textbf{Equation 6.5}$$

The correlation coefficient for this equation is 0.9894.

Although the correlation coefficient is very high, there are still observable differences between the contour plots seen in Figure 6.4a and Figure 6.4b. Like the Sinuosity best-fit surface, at low amplitude and frequency combinations there is a gentle increase in roughness indices that are not present on the Modified Divider a-Value roughness indices contour plot. The location of

the 3.0 level contour line is different between the original roughness indices and the best-fit surface contour plot.

In general, the best-fit surface accurately represents the roughness indices at frequencies greater than 0.5 Hz and amplitudes greater than 1 mm, as shown in the percent difference contour plot (Figure 6.4c). There were no percentage differences greater than 5% so a 0.5% contour was chosen and values greater than 0.5% are highlighted. The area that is highlighted on this plot is very small meaning that the equation satisfies almost all combinations of amplitude and frequency. The approximate planar area below the 0.5% contour is 94.84% indicating that the best-fit surface adequately represents approximately 95% of the roughness indices.

The best-fit surfaces for Sinuosity and Modified Divider a-Value had difficulty predicting roughness values at very low amplitudes and frequencies. Even with this limitation, both best-fit surfaces represented the roughness indices very well. For the Sinuosity best-fit surface, approximately 95% of the roughness indices are predicted to be within 5% of their actual values. For the Modified Divider a-Value best-fit surface, approximately 95% of the roughness indices are predicted to be within 0.5% of their actual values.

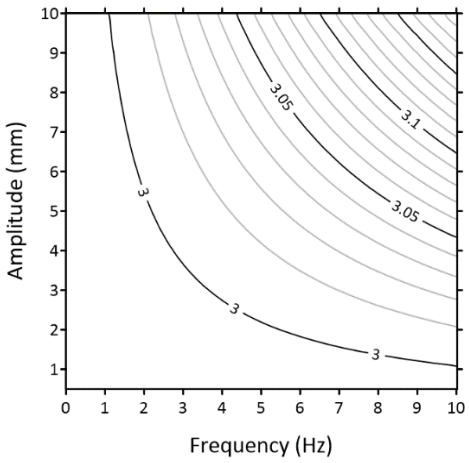

Figure 6.4a: Modified Divider a-Value Roughness Indices Contour Plot

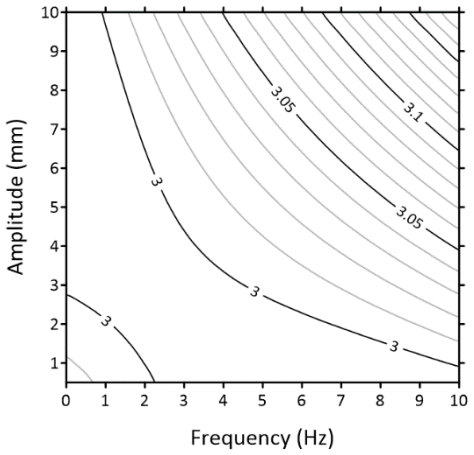

Figure 6.4b: Best-fit Surface for Modified Divider a-Value Roughness Indices

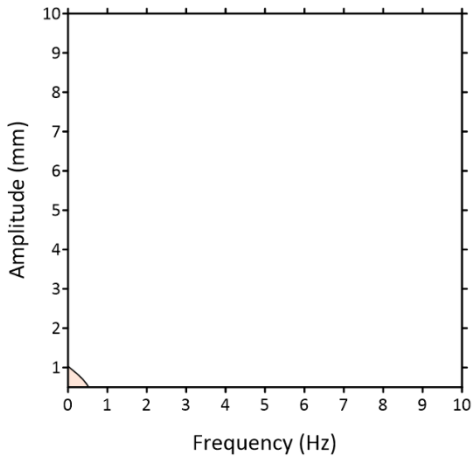

Figure 6.4c: Percentage Difference Modified Divider a-Value Contour Plot with 0.5% Tolerance Contour

Figure 6.4 Contour Plots of Modified Divider Roughness Indices, Fitted Surface to the Roughness Indices, and the Percent Difference Between Roughness Indices and the Fitted Surface.

6.1.3 Best-Fit Surfaces for Z2 and MAA Roughness Indices

Figure 6.5 shows the contour plots for the Z2 roughness indices (Figure 6.5a), the best-fit surface for the roughness indices (Figure 6.5b), and the percentage difference contour plot between the roughness indices and the best-fit surface (Figure 6.5c). The equation for the best-fit surface is:

$$z_{Z2} = -5.366 \times 10^{-5} + 6.604 \times 10^{-5}x + 3.688 \times 10^{-6}y - 1.659 \times 10^{-5}x^2 + 3.863 \times 10^{-11}y^2 + 0.0123xy + 1.106 \times 10^{-6}x^3 - 8.397 \times 10^{-11}y^3 + 2.984 \times 10^{-10}xy^2 + 1.595 \times 10^{-6}x^2y \quad \textbf{Equation 6.6}$$

The correlation coefficient for the equation is 0.9999.

The contour plots in Figure 6.5a and Figure 6.5b are almost identical. Visually, there are no noticeable differences between the plots. Both plots show a power curve trend, and the same maximum contour line is present in the upper right-hand corner of the plot.

In general, the best-fit surface accurately represents the roughness indices at frequencies greater than 1 Hz, as shown in the percent difference contour plot (Figure 6.5c). The percentage difference of 5% is shown and percentage differences greater than 5% are highlighted. There is a series of ovals along a frequency of 1 Hz. The approximate planar area below the 5% contour is 93.62% indicating that the best-fit surface adequately represents approximately 94% of the roughness indices.

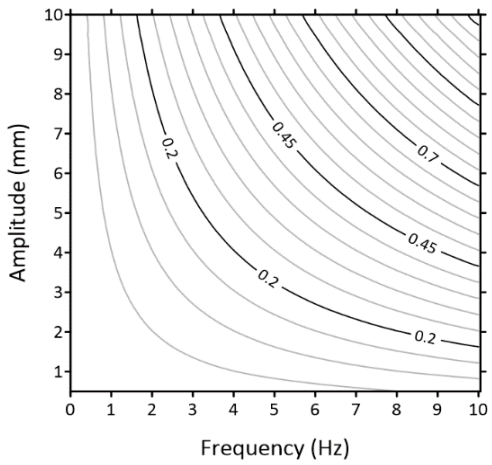

Figure 6.5a: Z2 Roughness Indices Contour Plot

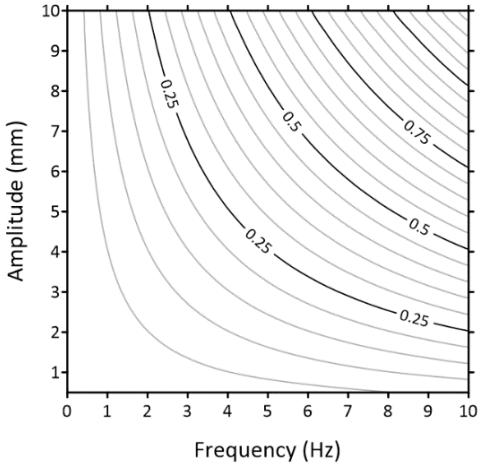

Figure 6.4b: Best-fit Surface for Z2 Roughness Indices

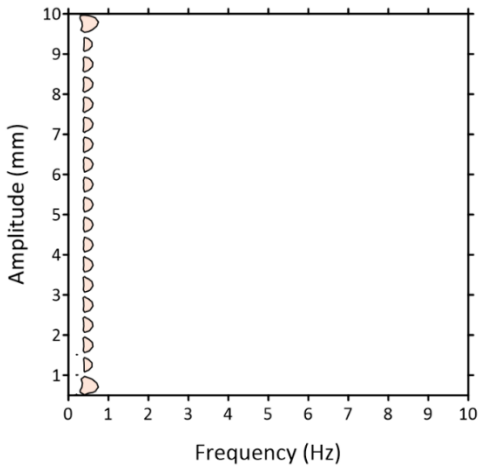

Figure 6.5c: Percent Difference Z2 Contour Plot with 5% Tolerance Contour
Figure 6.5 Contour Plots of Z2 Roughness Indices, Fitted Surface to the Roughness Indices, and the Percent Difference Between Roughness Indices and the Fitted Surface.

Figure 6.6 shows the contour plots for the MAA roughness indices (Figure 6.6a), the best-fit surface for the roughness indices (Figure 6.6b), and the percentage difference contour plot between the roughness indices and the best-fit surface (Figure 6.6c). The equation for the best-fit surface is:

$$z_{MAA} = 0.01579 + 0.01x + 0.009y + 0.0011x^2 + 0.0009y^2 + 0.0165xy - 1.123 \times 10^{-7}x^3 - 8.535 \times 10^{-6}y^3 - 0.0004xy^2 - 0.0004x^2y \qquad \textbf{Equation 6.7}$$

The correlation coefficient for the equation is 0.9998.

Although the correlation coefficient is very high, there are some evident differences between the contour plots in Figure 6.6a and Figure 6.6b. There is a contour line present along the frequency axis of the best-fit surface. This contour causes the following contours to be more compressed than the contours of the roughness indices.

In general, the best-fit surface accurately represents the roughness indices at frequencies greater than 2 Hz and amplitudes greater than 2 mm, as shown in the percent difference contour plot (Figure 6.5c). The percentage difference of 5% is shown and percentage differences above

5% are highlighted. The differences occur in an L-shaped region bounded by a frequency of 1.5 Hz and amplitudes less than 1.5 mm. The approximate planar area below the 5% contour is 82.79% indicating that the best-fit surface adequately represents approximately 83% of the roughness indices.

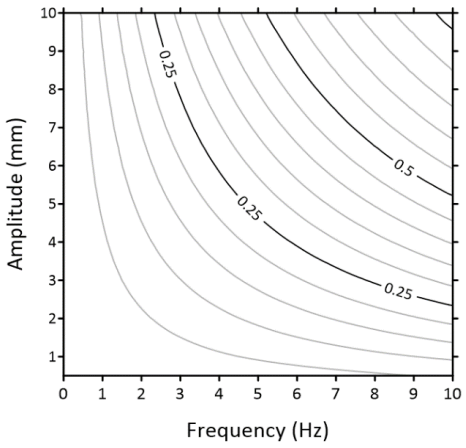

Figure 6.6a: MAA Roughness Indices Contour Plot

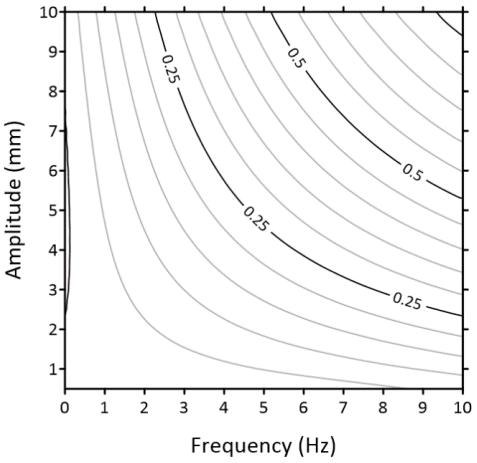

Figure 6.6b: Best-fit Surface for MAA Roughness Indices

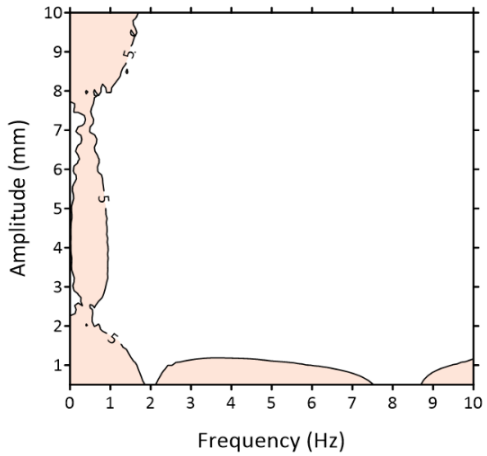

Figure 6.6c: Percent Difference MAA Contour Plot with 5% Tolerance Contour
Figure 6.6 Contour Plots of MAA Roughness Indices, Fitted Surface to the Roughness Indices, and the Percent Difference Between Roughness Indices and the Fitted Surface.

The Z2 roughness indices can be much better represented by a best-fit surface than the MAA roughness indices. The best-fit surface for the Z2 roughness indices is almost identical to the roughness indices plot, whereas in the MAA best-fit surface, an additional contour line is present along the frequency axis. This additional contour caused a large percentage difference at low frequencies.

Table 6.1 highlights the locations, in terms of amplitude and frequency, where the best-fit surface equations have a poor fit to the roughness indices for each of the roughness algorithms. The A poor fit has been defined as a percentage difference greater than 5%. These locations were also seen as highlighted in pink on each of the percentage difference plots.

Table 6.1 Summary of Locations of Poor Fit to Roughness Indices

Roughness Algorithm	Location of Insensitivity using Combinations of Amplitude and Frequency
Root Mean Square (RMS)	• Frequencies less than 1 Hz for all amplitudes • Frequencies between 0-5.5 Hz for amplitudes less than 3.5 mm

	• Frequencies between 6.5-10 Hz for amplitudes less than 4mm
Energy	• Frequencies less than 0.5 Hz for all amplitudes • Frequencies between 0-5.25 Hz for amplitudes less than 2 mm • Frequencies between 5.75-10 Hz for amplitudes less than 2 mm
Sinuosity	• Frequencies less than 0.5 Hz for amplitudes less than 1 mm
Modified Divider a-Value	• Frequencies less than 0.5 Hz for amplitudes less than 1 mm
Z2	• Frequencies less than 1 Hz for all amplitudes
Mean Absolute Angle (MAA)	• Frequencies less than 1 Hz for all amplitudes • Frequencies between 0-2 Hz for amplitudes between 0-2 mm • Frequencies between 0-2 Hz for amplitudes between 8-10 mm • Frequencies between 2-7.5 Hz for amplitudes less than 1.5 mm • Frequencies between 9-10 Hz for amplitudes less than 1 mm

6.2 Equations Linking Roughness Algorithms

The six roughness equations have been paired: Energy and Root Mean Square, Z2 and Mean Absolute Angle, and Modified Divider a-Value and Sinuosity. The linking equations were developed using a four-step process. First, a translation factor was computed using the higher value roughness indices divided by the lower value roughness indices for the paired algorithms. A best-fit surface was then fitted to the translation factor. Then a computed roughness value was computed for the higher value roughness indices using the best-fit surface equation and the roughness indices from the lower values roughness algorithm. Finally, a percentage difference

was calculated between the roughness indices and the computed roughness indices. To visualize the success of the linking equation, contour plots of the percentage difference value, with a tolerable error of 5%, was produced. The step-by-step process for each pair of roughness algorithms is outlined below:

- Compute the translation factors using the following relationships:

$$Translation\ Factor_{Energy:RMS} = \frac{Energy_{indices}}{RMS_{indices}} \quad \textbf{Equation 6.}8a$$

$$Translation\ Factor_{Z2:MAA} = \frac{Z2_{indices}}{MAA_{indices}} \quad \textbf{Equation 6.8b}$$

$$Translation\ Factor_{MDa:Sinuosity} = \frac{Modified\ Divider\ a\ Value_{indices}}{Sinuosity_{indices}} \quad \textbf{Equation 6.8c}$$

- Fit a surface to the Translation Factor.
- Use the best-fit surface to the Translation Factor equation (TF_{bfs}) to compute roughness indices:

$$Energy_{computed} = TF_{bfs\_Energy:RMS} \times RMS_{indices} \quad \textbf{Equation 6.9a}$$

$$Z2_{computed} = TF_{bfs\_Z2:MAA} \times MAA_{indices} \quad \textbf{Equation 6.9b}$$

$$MD\ a\ Value_{computed} = TF_{bfs\_ZMDa:Sinuosity} \times Sinuosity_{indices} \quad \textbf{Equation 6.9b}$$

- Determine the percentage difference between the roughness indices and the computed roughness indices:

$$Percent\ Difference = \frac{\left|Energy_{indices} - Energy_{computed\ indices}\right|}{\left|\frac{Energy_{indices} - Energy_{computed\ indices}}{2}\right|} \times 100 \quad \textbf{Equation 6.10a}$$

$$Percent\ Difference = \frac{\left|Z2_{indices} - Z2_{computed\ indices}\right|}{\left|\frac{Z2_{indices} - Z2_{computed\ indices}}{2}\right|} \times 100 \quad \textbf{Equation 6.10b}$$

$$Percent\ Difference = \frac{|MDa\ Value_{indices} - MD\ a\ Value_{computed\ indices}|}{\left|\frac{MDa\ Value_{indices} - MD\ a\ Value_{computed\ indices}}{2}\right|} \times 100$$ **Equation 6.10c**

- Develop a contour plot of the percentage differences and identify the locations where the percentage difference is greater than 5%.

6.2.1 Equation Relating Energy and RMS

The step-by-step process described above was applied to the roughness indices for Energy and RMS algorithms. The equation for the Translation Factor of the best-fit surface (TF_{bfs}) Energy and RMS is:

$$TF_{bfsEnergy:RMS} = 0.0917 - \frac{0.4079}{x} + 0.7015y + \frac{0.1705}{x^2} + 7.231 \times 10^{-9}y^2 + \frac{0.0074y}{x} - \frac{0.0132}{x^3} - 3.96 \times 10^{-10}y^3 - \frac{3.68*10^{-11}y^2}{x} + \frac{0.0103y}{x^2}$$ **Equation 6.11**

The correlation coefficient for the best-fit surface is 0.9965.

The translation factor equation was multiplied by the RMS roughness indices, which provided the computed Energy roughness indices. The percentage difference between the Energy roughness indices and computed Energy roughness indices was computed and visualized as a contour plot. Within the contour plot, the tolerable percentage difference of 5% is highlighted. The contour plot is shown in Figure 6.7.

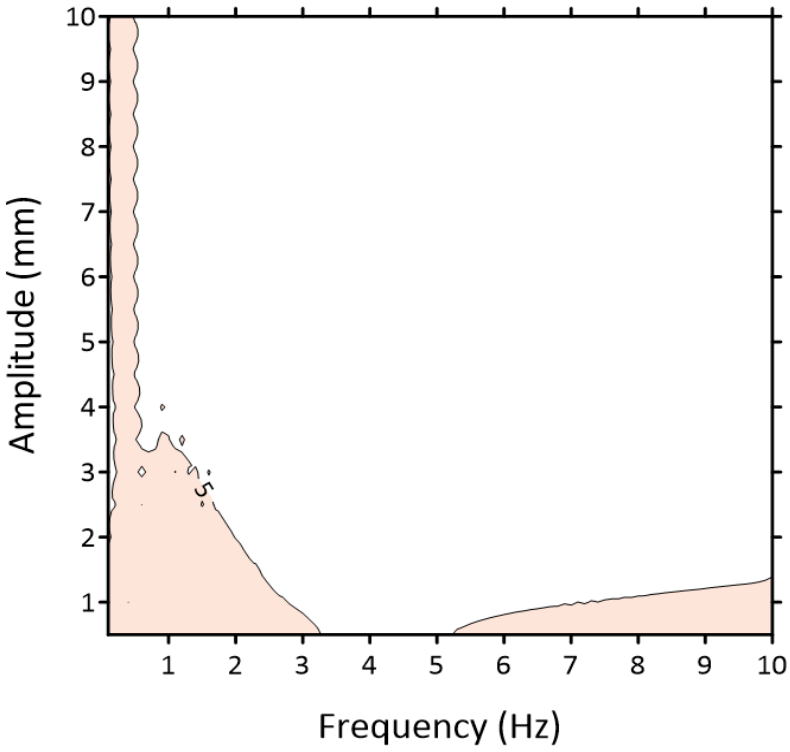

Figure 6.7 Contour of Five Percentage Difference between Energy Roughness Indices and Energy Roughness Indices computed from RMS Roughness Indices

The developed equation fails to capture the translation of Energy roughness indices based on the RMS roughness algorithm at frequencies below 1 Hz at all amplitudes. There are two other zones where the equation does not perform satisfactorily, at high frequencies and low amplitudes and at low amplitudes and low frequencies. Overall, the procedure accurately predicts the Energy roughness indices based on RMS roughness indices. Approximately 83 percent of the Energy roughness indices can be predicted from RMS roughness indices with a tolerable percentage difference of 5%.

6.2.2 Equation Relating Z2 and MAA

The step-by-step process described above was applied to the roughness indices for Z2 and MAA. The equation for the Translation Factor for the best-fit surface (TF_{bfs}) for Z2 and MAA is:

$$TF_{bfs_{Z2:MAA}} = 1.0512 + 0.02696\ln(x) - 0.6098(\ln(x))^2 + 0.00969(\ln(x))^3 + 0.0325(\ln(x))^4 - 0.0092(\ln(x))^5 - 0.00026y + 0.002747y^2 - 6.9256 \times 10^{-5}y^3 - 3.1372 \times 10^{-6}y^4 + 1.8979 \times 10^{-7}y^5 \quad \textbf{Equation 6.12}$$

The correlation coefficient for the best-fit surface is 0.8636.

The translation factor equation was multiplied by the MAA roughness indices, which provided the computed Z2 roughness indices. The percentage difference between the Z2 roughness indices and the computed Z2 indices was computed and visualized as a contour plot. Within this contour plot, the tolerable percentage difference of 5% is highlighted to show the goodness of fit. This contour plot is seen in Figure 6.8.

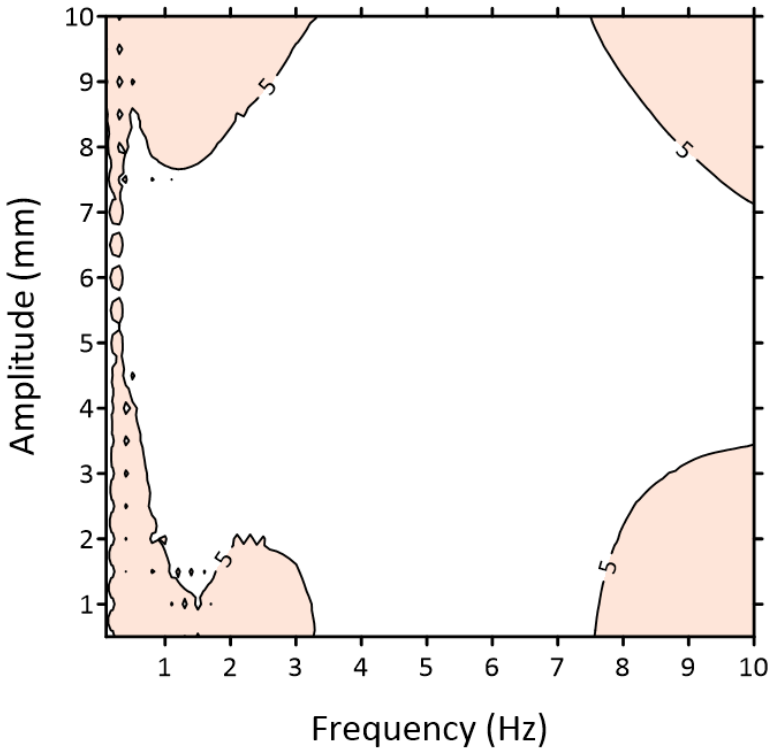

Figure 6.8 Contour of Five Percentage Difference Between Z2 Roughness Indices and Z2 Roughness Indices Computed from MAA Roughness Indices

The developed equation fails to capture the translation of Z2 roughness indices based on the MAA roughness indices at the four extreme locations within the ranges of amplitude and frequency. The equation fails to satisfactorily Z2 roughness values based on MAA roughness values at combinations of low frequency and high amplitude, low frequency and low amplitude, high frequency and high amplitude, and high amplitude and high frequency. The shapes of the zones where there is a greater than five percentage difference are non-symmetrical and cover different planar areas of the contour plot. Overall, the procedure can accurately predict the Z2 roughness indices based on the MAA roughness indices. Approximately 74 percent of the Z2 roughness indices can be predicted from the MAA roughness indices with a tolerable percentage difference of 5%.

6.2.3 Equation Relating Modified Divider a-Value and Sinuosity

The step-by-step process described above was applied to the roughness indices for Modified Divider a-Value and Sinuosity algorithms. The equation for the best-fit surface (*bfs*) for the translation factor (*TF*) between Modified Divider a-Value and Sinuosity is:

$$TF_{bfs\_MDaValue:Sinuosity} = 2.899 + 0.04048x + 0.03686y - 0.00257x^2 - 0.00227y^2 - 0.01145xy \quad \textbf{Equation 6.13}$$

The correlation equation for the best-fit surface is 0.9927.

The translation factor equation was multiplied by the Sinuosity roughness indices, which provided the computed Modified Divider a-Value roughness indices. The percentage difference between the Modified Divider a-Value roughness indices and the computed Modified Divider a-Value roughness indices was computed and visualized as a contour plot. Within this contour plot, the tolerable percentage difference of 1% was chosen because of the excellent match between the real and computed Modified Divider a-Values. The 1% percentage difference can be seen in the contour plot in Figure 6.9.

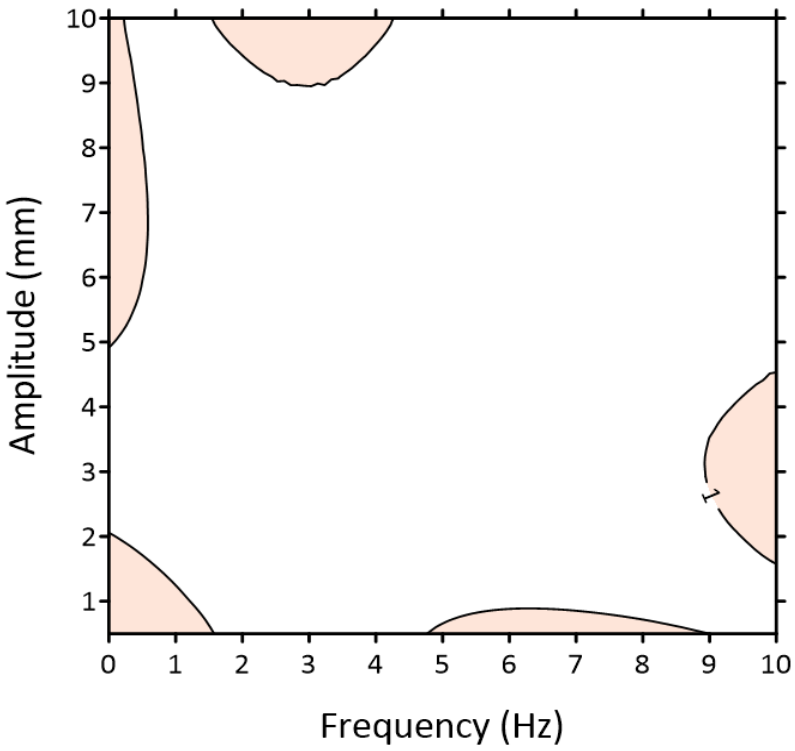

Figure 6.9 Contour of One Percentage Difference between Modified Divider a-Values and Modified Divider a-Values computed from Sinuosity Roughness Indices

The developed equation fails to capture the translation of Modified Divider a-Value roughness indices based on the Sinuosity roughness indices at small but very specific locations. The locations in which the translation equation may not accurately capture the data are in locations where: the combination of amplitude is less than 2 mm and less than 1.5 Hz, at very low amplitudes for frequencies between 5 and 9 Hz, at very low frequencies with amplitudes between 5 and 10 mm, at amplitudes greater than 8 mm and frequencies between 2.5 and 5.5 Hz, and at frequencies greater than 9 Hz and amplitudes between 1.5 and 4.5 mm. To reiterate, the percentage difference used for this relation is a 1% difference which tells us that the fit of this translation equation is much greater than the fit of the others. Overall, the procedure accurately predicts the Modified Divider a-Value roughness indices based on Sinuosity roughness indices. Approximately 86 percent of the Modified Divider a-Value roughness indices can be predicted from Sinuosity roughness indices with a tolerable percentage difference of 1%.

6.3 Chapter Summary

Best-fit surfaces have been successfully fit to the roughness indices for each roughness algorithm. The form of the equation for the best-fit surface was chosen to be a polynomial. The correlation coefficients for all best-fit surfaces were greater than 0.98. The best-fit surface roughness indices were compared to the roughness indices to assess the goodness of fit. A tolerable percentage difference of 5% was used. The planar area of the contour plots with less than 5% difference ranged between 71.9% and 94.9% for Energy, RMS, Sinuosity, MAA, and Z2. The planar of the contour plot with less than 0.5% difference for Modified Divider a-Value was 94.8%.

A procedure to develop an equation linking the paired algorithms was developed. The paired algorithms are Energy and Root Mean Square, Z2 and MAA, and Modified Divider a-Value and Sinuosity. First a translation factor was computed by dividing the larger roughness indices by the smaller roughness indices. A best-fit surface and associated equation was then determined. The correlation coefficient for the translation factors ranged between 0.8636 (Z2 and MAA) and 0.9965 (Energy and RMS). The computed roughness indices of the algorithm with the largest roughness indices were computed by multiplying translation factor by the smaller roughness indices. The percentage difference between the roughness indices and the computed roughness indices was calculated and assessed using a 5% tolerable difference. The planar area of the contour plots with less than five percent difference ranged between 73.8% (Z2 and MAA) and 83.3% (Energy and RMS). The equation linking Sinuosity and Modified Divider a-Value worked so well that there was no area in the contour plot that corresponded to a 5% tolerable difference. The planar area of the contour plot showing 1% tolerable difference for Sinuosity and Modified Divider a-Value was 86.2%.

CHAPTER SEVEN: SUMMARY AND FUTURE WORK

7.1 Summary

This thesis presented a systemic investigation to quantify the effect of amplitude and frequency on the roughness indices of simulated wavy profiles using six common roughness algorithms. The simulated wavy profiles were created using sine waves of amplitudes between 0 and 10 mm with a step size of 0.1 mm and frequencies between 0 and 10 Hz with a step size of 0.5 Hz. Four research questions were posed at the beginning of the thesis.

- Is it possible to visualize roughness indices as a function of amplitude and frequency?
- How does systematically changing the amplitude and frequency of a sine wave profile affect the roughness index of a given roughness algorithm?
- Is it possible to establish a comparative relationship between the roughness indices of different algorithms?
- Is it possible to develop equations to relate the roughness indices of roughness algorithms?

To visualize the roughness indices as a function of amplitude and frequency, roughness indices were plotted as a function of amplitude (x-axis) and frequency (y-axis) in a contour plot. Cross-sections were taken at different locations on these contour plots. which created new profiles that allowed for the investigation of the effects of the amplitude and frequency. For the RMS and Energy algorithms, cross-sections were taken at a constant amplitude or a constant frequency and this allowed for the effects of changing one parameter to be analyzed. For the other algorithms, the cross-sections were taken from a 45-degree line from the origin to an amplitude of

10 mm and a frequency of 10 Hz. This allowed the determination of the effects of the paired combinations of amplitude and frequency on the roughness index. At a constant frequency, the RMS roughness index increased linearly with the increase of amplitude, but all other roughness indices increased non-linearly with the increase of amplitude, frequency, or a paired combination of both.

Observations were made on the behaviors of the contour plots for each of the roughness algorithms. These plots show that it is easy to determine that these algorithms behave similarly to one another. Roughness algorithms were grouped together based on their contour shape, the magnitude of the contours, and the spacing of the contours. Two apparent groups were created, with the first group contained RMS and Energy and the second group contained Sinuosity, Z2, MAA, and Modified Divider a. The comparison and differences of each of the contour plots were discussed and this information helped lead into the relating of one algorithm to another.

The contour plots created by each algorithm can also be termed as surfaces and to represent these surfaces of data, equations were found to represent them. Best-fit equations were applied to the surfaces created by the data from the roughness algorithms and an equation was chosen based on the simplicity and high correlation coefficient. The percentage difference was found between the best-fit computed roughness indices and the roughness algorithm roughness indices. The percentage difference was used to validate the strength of the best-fit equation as well as highlight regions where the equation may not be strong. The best-fit surface equation was found to express the roughness algorithms in another way as well as validate a procedure for determining a best-fit surface. The correlation coefficients from the chosen best-fit surface equations ranged from 0.9825 to 0.9999. With a 5-percentage difference tolerable contour, the equations accurately represented more than 72% of the roughness index data.

Translation factors between the paired roughness algorithms were found and a best-fit surface equation representing these factors was determined. A 1-percentage difference and a 5-

percentage difference were used to represent the strength of fit and locations of where the equation is not satisfied. For the equation relating the roughness indices of RMS and Energy, the correlation coefficient was 0.9965 it was concluded that 83 percent of the Energy roughness indices can be predicted from RMS roughness indices with a tolerable percentage difference of 5%. For the equation relating the roughness indices of Z2 and MAA, the correlation coefficient was 0.8636 and it was concluded that 74 percent of the Z2 roughness indices can be predicted from the MAA roughness indices with a tolerable percentage difference of 5%. Lastly, for the equation relating the roughness indices of Modified Divider a-Value and Sinuosity, the correlation coefficient was 0.9927 and it was concluded that 86 percent of the Modified Divider a-Value roughness indices can be predicted from Sinuosity roughness indices with a tolerable percentage difference of 1%. Overall, it was determined that equations can be generated to accurately relate the roughness indices of one roughness algorithms to another.

The significance of this work is that it furthers the understanding of roughness by assessing the changes in roughness indices of symmetrical smooth profiles based on a single sine wave. The amplitude and frequency of the sine wave were systematically increased to assess the changes in roughness indices. Determining the influences of amplitude and frequency on a roughness index will help aid in the visualization of rock joints and how much this will affect its shear strength. The development of equations is another significant portion, showing it is possible to relate one roughness index to another while preserving the influence of amplitude and frequency.

7.2 Future Work

This thesis was focused on using sine wave based wavy synthetic profiles to investigate the effect of systematically changing amplitude (between 0 and 10 mm) and frequency (between 0 and 10 Hz) on the roughness indices. Prior work has indicated that waviness is present on a decimeter to meter scale and unevenness is present on a millimeter and centimeter scale. My

research took a slightly different approach and defined waviness as the absence of small-scale perturbations superimposed on smooth profiles consisting of single amplitude and frequency sine waves. Along this theme, several new line of inquiry should be undertaken. These include:

- Continue to use wavy profiles as defined in this thesis but incorporate the traditional frequency-based definitions of waviness and unevenness and add a new definition of amplitude-based waviness and unevenness.
- Increase the complexity of the simulated profiles by superimposing multiple waves of single amplitudes and frequencies.
- The amplitude bounds used in this study are realistic, but frequency bounds could be extended for a new study.
- Potentially improving the mathematical relationships identified between some of the paired algorithms by using piece-wise defined best-fit equations. One equation should represent the low frequency component and a different equation should represent the high frequency component.

The Joint Roughness Coefficient is still widely used in engineering practice to incorporate roughness into rock shear strength. A next step in the investigation of amplitude and frequency could be relating the algorithms and roughness indices to JRC values. This would extend the applicability of the research because practitioners are more familiar with JRC than roughness algorithms.

Finally, another potential for future work could be extending the investigation by incorporating more roughness algorithms. Additional two-dimensional algorithms and potentially three-dimensional algorithms could be used.

REFERENCES

Ankah, M. L. Y., Sunkpal, D. T., & Zhao, X. (2021). Quantification of joint roughness using various empirical relations between JRC and roughness parameters. *IOP Conference Series*, *861*(5), 052052. https://doi.org/10.1088/1755-1315/861/5/052052

Asadi, M. B., Rasouli, V., & Barla, G. B. (2012). A bonded particle model simulation of shear strength and asperity degradation for rough rock fracture. *Rock Mechanics and Rock Engineering*. https://doi.org/10.1007/s00603-012-0231-4

ASTM Standard D4543-19. (2019). Standard Practices for Preparing Rock Core as Cylindrical Test Specimens and Verifying Conformance to Dimensional and Shape Tolerances, ASTM International.

Barton, N. R. (1973). Review of a new shear-strength criterion for rock joints. *Engineering Geology*, *7*(4), 287–332. https://doi.org/10.1016/0013-7952(73)90013-6

Barton, N. R., & Choubey, V. (1977). The shear strength of rock joints in theory and practice. *Rock Mechanics*, *10*(1–2), 1–54. https://doi.org/10.1007/bf01261801

Barton, N.R., (1981). *Shear strength investigation for surface mining*. In: Proceedings of the 3rd International Conference on Surface Mining. SME, Vancouver.

Beer, A. J., Stead, D., & Coggan, J. (2002). Estimation of the joint roughness coefficient (JRC) by visual comparison. *Rock Mechanics and Rock Engineering*, *35*(1), 65–74. https://doi.org/10.1007/s006030200009

Benson, R., Sroka, G., & Bell, M. (2013) The effect of the Surface Roughness Profile on Micropitting. GearSolutions.com.

Brown, S. J. (1987). A note on the description of surface roughness using fractal dimension. *Geophysical Research Letters*, *14*(11), 1095–1098. https://doi.org/10.1029/gl014i011p01095

Brown, S. K. Ball, L. Kimes, J. Oglesby, A. Harris, & Hudyma, N, (2016). Sensitivity of roughness algorithms to sampling frequency for the characterization of weathered limestone cores. 50th US Rock Mechanics/Geomechanics Symposium, Houston, 26-29 June 2016.

Candela, T., Renard, F., Bouchon, M., Brouste, A., Marsan, D., Schmittbuhl, J., & C, V. (2009). Characterization of fault roughness at various scales: implications of three-dimensional high resolution topography measurements. Pure and Applied Geophysics, 166, 1817-1857. https://doi.org/ 10.1007/s00024-009-0521-2

Cox, B. L., & Wang, J. (1993). Fractal surfaces: measurement and applications in the earth sciences. *Fractals*, *01*(01), 87–115. https://doi.org/10.1142/s0218348x93000125

Develi, K., & Babadagli, T. (1998). Quantification of natural fracture surfaces using fractal geometry. *Mathematical Geosciences*, *30*(8), 971–998. https://doi.org/10.1023/a:1021781525574

Dong, S., Zhang, H., Peng, Y., Lu, Z., & Hou, W. (2022). Method of calculating shear strength of rock mass joint surface considering cyclic shear degradation. *Scientific Reports*, *12*(1). https://doi.org/10.1038/s41598-022-13505-6

Fecker, E. and Rengers, N.F. (1971). *Measurement of large -scale roughness of rock planes by means of profilograph and geological compass.* 1st ISRM Symposium on Rock Fracture, Nancy, France, 4-6 October 1971.

Ge, Y., Kulatilake, P. H., Tang, H., & Xiong, C. (2014). Investigation of natural rock joint roughness. *Computers and Geotechnics*, *55*, 290–305. https://doi.org/10.1016/j.compgeo.2013.09.015

Goehring, L., Nakahara, A., Dutta, T., Kitsunezaki, S., & Tarafdar, S. (2015). *Desiccation Cracks and their Patterns: Formation and Modelling in Science and Nature*. John Wiley & Sons.

Guo, Y., Zhang, C., Xiang, H., Guojian, C., Meng, F., & Zhou, H. (2022). Quantitative characterization method for rock surface roughness with difference scale fluctuation *KSCE Journal of Civil Engineering*, *26*(4), 1695–1711. https://doi.org/10.1007/s12205-022-1228-5

Greene, S., Akbarian, M., Ulm, F., & Gregory, J. (2013). Pavement Roughness and Fuel Consumption. Concrete Sustainability hub. Cshub.mit.edu.

Huang, S., Oelfke, S. R., & Speck, R. (1992). Applicability of fractal characterization and modelling to rock joint profiles. *International Journal of Rock Mechanics and Mining Sciences & Geomechanics Abstracts*, *29*(2), 89–98. https://doi.org/10.1016/0148-9062(92)92120-2

Jang, H., Kang, S., & Jang, B. (2014). Determination of joint roughness coefficients using roughness parameters. *Rock Mechanics and Rock Engineering*, *47*(6), 2061–2073. https://doi.org/10.1007/s00603-013-0535-z

Kadivar, M., Tormey, D., & McGranaghan, G. (2021). A review on turbulent flow over rough surfaces: Fundamentals and theories. *International Journal of Thermofluids*, *10*, 100077. https://doi.org/10.1016/j.ijft.2021.100077

Kim, D. H., Gratchev, I., & Poropat, G. (2013). *The determination of joint roughness coefficient using three-dimensional models for slope stability analysis*. 2013 International Symposium on Slope Stability in Open Pit Mining and Civil Engineering. https://doi.org/10.36487/ACG_rep/1308_15_Kim

Klinkenberg, B., & Goodchild, M. F. (1992). The fractal properties of topography: a comparison of methods. *Earth Surface Processes and Landforms*, *17*(3), 217–234. https://doi.org/10.1002/esp.3290170303

Li, Y., & Zhang, Y. (2015). Quantitative estimation of joint roughness coefficient using statistical parameters. *International Journal of Rock Mechanics and Mining Sciences*, *77*, 27–35. https://doi.org/10.1016/j.ijrmms.2015.03.016

Luo, S., Zhao, Z., Peng, H., & Pu, H. (2016). The role of fracture surface roughness in macroscopic fluid flow and heat transfer in fractured rocks. *International Journal of Rock Mechanics and Mining Sciences*, *87*, 29–38. https://doi.org/10.1016/j.ijrmms.2016.05.006

Maerz, N. H., Franklin, J. H., & Bennett, C. P. (1990). Joint roughness measurement using shadow profilometry. *International Journal of Rock Mechanics and Mining Sciences & Geomechanics Abstracts*, *27*(5), 329–343. https://doi.org/10.1016/0148-9062(90)92708-m

Mandelbrot, B. B. (1983). *The Fractal Geometry of Nature*. Times Books.

McCarroll D. and A. Nesje. (1996). Rock surface roughness as an indicator of degree of rock surface weathering. *Earth Surface Processes and Landforms*. 21: 10, 963-977. https://doi.org/10.1002/(SICI)1096-9837(199610)21:10<963::AID-ESP643>3.0.CO;2-J

McGough, M., Kimes, L., Harris, A., Kreidl, O. P., & N. Hudyma. (2015). *Investigation of roughness algorithms applied to JRC profiles for assessment of weathering*. 49th U.S. Rock Mechanics/Geomechanics Symposium, San Francisco, California, June 2015.

Milne, D., Germain, P., Grant, D. & Noble, P. (1991). *Field observation for the standardization of the NGI classification system for underground mine design*. International Congress on Rock Mechanics, A.A. Balkema, Aachen, Germany.

McKillup, S., & Dyar, M. D. (2010). *Geostatistics Explained: An Introductory Guide for Earth Scientists*. Cambridge University Press.

Newland, P. L., & Allely, B. H. (1957). Volume changes in drained triaxial tests on granular materials. *Geotechnique*, *7*(1), 17–34. https://doi.org/10.1680/geot.1957.7.1.17

Nyende-Byakika, S. (2017). Impact of pipe roughness on the performance of a water distribution network: A case study of the Westbury Network, Johannesburg, South Africa. *African Journal of Science, Technology, Innovation and Development*. https://doi.org/10.1080/20421338.2017.1289648

Oliver, M. A., & Webster, R. D. (2015). *Basic Steps in Geostatistics: The Variogram and Kriging*. Springer International Publishing. https://doi.org/10.1007/978-3-319-15865-5

Pagliara, S., & Carnacina, I. (2010). Temporal scour evolution at bridge piers: effect of wood debris roughness and porosity. *Journal of Hydraulic Research*, *48*(1), 3–13. https://doi.org/10.1080/00221680903568592

Patton, F. D. (1966). Multiple modes of shear failure in rock. *Journal of Geophysical Research*, 71(12), 3077-3094.

Poropat, G. V. (2009). *Measurement of Surface Roughness of Rock Discontinuities*. RockEng09 – 3rd Canada-US Rock Mechanics Symposium & 20th Canadian Rock Mechanics Symposium, Toronto, ON, Canada.

Rasouli, V., & Harrison, J. P. (2010). Assessment of rock fracture surface roughness using Riemannian statistics of linear profiles. *International Journal of Rock Mechanics and Mining Sciences*, *47*(6), 940–948. https://doi.org/10.1016/j.ijrmms.2010.05.013

Saadat, M., & Taheri, A. (2020). A numerical study to investigate the influence of surface roughness and boundary condition on the shear behaviour of rock joints. *Bulletin of Engineering Geology and the Environment*, *79*(5), 2483–2498. https://doi.org/10.1007/s10064-019-01710-z

Saleh, A. (1993). Soil roughness measurement: Chain method. *Journal of Soil and Water Conservation*, 48, 527-529

Stigsson, M., & Ivars, D. M. (2019). A novel conceptual approach to objectively determine JRC using fractal dimension and asperity distribution of mapped fracture traces. *Rock Mechanics and Rock Engineering*, *52*(4), 1041–1054. https://doi.org/10.1007/s00603-018-1651-6

Tatone, B. S. A., & Grasselli, G. (2013). An investigation of discontinuity roughness scale dependency using high-resolution surface measurements. *Rock Mechanics and Rock Engineering*, *46*(4), 657–681. https://doi.org/10.1007/s00603-012-0294-2

Tse, R., & Cruden, D. (1979). Estimating joint roughness coefficients. *International Journal of Rock Mechanics and Mining Sciences & Geomechanics Abstracts*, *16*(5), 303–307. https://doi.org/10.1016/0148-9062(79)90241-9

Vuopio, J., & Pöllä, J. (1997). Characterization of the rock surface. Helsinki: STUK.

Xuezhen, W., Zheng, H., & Jiang, Y. (2022). Study on the evolution law of rock joint shear stiffness during shearing process through loading-unloading tests. *Tunnelling and Underground Space Technology*, *127*, 104584. https://doi.org/10.1016/j.tust.2022.104584

Yang, Z., Di, C. C., & Yen, K. C. (2001). The effect of asperity order on the roughness of rock joints. *International Journal of Rock Mechanics and Mining Sciences*, *38*(5), 745–752. https://doi.org/10.1016/s1365-1609(01)00032-6

Yang, Z. Y., Taghichian, A., & Li, W. C. (2010). Effect of asperity order on the shear response of three-dimensional joints by focusing on damage area. *International Journal of Rock Mechanics and Mining Sciences*, 47, 1012-1026. https://doi.org/10.1016/ j.ijrmms.2010.05.008

Yuan, W., Liu, S., Hanhua, T., Niu, J., Zhiling, J., Xilai, L., Shu, P., Yanyu, X., Wang, W., & Xiaoyun, S. (2021). A new approach for quantifying the two-dimensional joint roughness coefficient (JRC) of rock joints. *Environmental Earth Sciences*, *80*(15). https://doi.org/10.1007/s12665-021-09780-7

Zareidoost, A., Yousefpour, M., Ghaseme, B., & Amanzadeh, A. (2012). The relationship of surface roughness and cell response of chemical surface modification of titanium. *Journal of Materials Science: Materials in Medicine*, *23*(6), 1479–1488. https://doi.org/10.1007/s10856-012-4611-9